Ore Geology Reviews 146 (2022) 104959

Contents lists available at ScienceDirect

Ore Geology Reviews

journal homepage: www.elsevier.com/locate/oregeorev

Heterogeneity of mineral chemistry and sulfur isotopic composition of alunite in the Mankayan lithocap, northern Luzon, Philippines

Pearlyn Manalo [a,b,*], Ryohei Takahashi [a], Akira Imai [c], Rhyza Ruth Parcon-Calamohoy [d], Mervin de los Santos [d,e], Leo Subang [d], Glenn Christian Alburo [d]

[a] Graduate School of International Resource Sciences, Akita University, 1-1 Tegatagakuenmachi, Akita City, Akita, Japan
[b] International Center for Research and Education on Mineral and Energy Resources, Akita University, 1-1 Tegatagakuenmachi, Akita City, Akita, Japan
[c] Faculty of Engineering, Kyushu University, 744 Motooka Nishi-ku, Fukuoka, Japan
[d] Lepanto Consolidated Mining Company, Makati City, Philippines
[e] FCF Minerals Corporation, Runruno, Quezon, Nueva Vizcaya, Philippines

ARTICLE INFO

Keywords:
Alunite
Natroalunite
High-sulfidation
Quartz-pyrite-gold
Sulfur isotopes
Mankayan
Luzon
Lepanto

ABSTRACT

The lithocap at Mankayan is a contiguous zone of alunite + quartz + pyrite that occur as pervasive alteration of the metavolcanic basement and dacitic pyroclastic rocks. Alunite + quartz + pyrite assemblage also occurs within hydrothermal gold-bearing veins and breccias. Several high-sulfidation epithermal gold orebodies have been previously delineated in the Lepanto Main Enargite orebody, and in the Northwest, Carmen, Florence West and Florence East quartz-pyrite-gold (QPG) veins. This study presents new data of mineral composition and sulfur isotopic ratios of alunites from different zones of the lithocap at Mankayan. Elemental composition maps and point analysis of alunites indicate compositional heterogeneity within a single alunite crystal. Common substituents to the K^+ site are Na^+ and H_3O^+, with few Ca^{2+} substitution in some sites. Limited occurrences of PO_4^{3-} substitution to SO_4^{2-} were also documented. Sulfur isotopic ratios ($\delta^{34}S_{CDT}$) of alunite range from + 13 ‰ to + 24 ‰, which are typical of hypogene alunite. Sulfur isotopic ratios of coexisting pyrite are mostly negative, ranging from −5.4 to −1.0 ‰. Few samples of alunite from the Northwest and Florence West quartz-pyrite-gold veins have sulfur isotopic ratios similar to the values of its coexisting pyrite. The estimated temperature of formation using sulfur isotope geothermometry of alunite-pyrite pairs ranges from 197 °C to 364 °C, with most of the samples varying within 220 to 270 °C. The calculated bulk $\delta^{34}S$ of the hydrothermal fluid was found to be + 5 to + 6 ‰ for the different mineralization events in Mankayan.

The alunite crystals are heterogeneous even in the microscopic scale. Compositional maps show that K and Na concentration vary within single crystals, as well as among different crystals of a sample. The variations of K and Na content mostly follow the crystal growth structure, however, some alunite crystals with irregular variations are also present. Some samples contain aluminum-phosphate-sulfate (APS) minerals intergrown with alunite. Electron probe microanalysis of the alunite crystals showed a generally wide range of composition between the alunite – natroalunite solid solution.

Using thermodynamic functions, a relationship between temperature and K^+/Na^+ of the hydrothermal fluids was determined across the range of alunite-natroalunite solid solution system. The model curves suggest that at temperatures less than ~ 250 °C a slight change in fluid composition and/or temperature can vary the number of Na atoms per formula unit by 0.3 units. At higher temperatures, a more significant change in the physico-chemical conditions is required for a substitution to occur. This explains the wide range of Na content in the alunites from the different parts of the lithocap.

The characteristics compiled in this study reflect the fluctuations in temperature and fluid compositions that occurred during the multiple hydrothermal events in the Mankayan District.

* Corresponding author.
E-mail address: pcmanalo@gipc.akita-u.ac.jp (P. Manalo).

https://doi.org/10.1016/j.oregeorev.2022.104959
Received 29 September 2021; Received in revised form 21 May 2022; Accepted 26 May 2022
Available online 28 May 2022

1. Introduction

Alunite is a sulfate mineral with a chemical composition of $KAl_3(SO_4)_2(OH)_6$ (Beudant, 1824; Bayliss et al., 2010; Back, 2014). It is also a name of a mineral group with a general composition of $DG_3(TO_4)_2(OH, H_2O)$, where D can be monovalent (K^+, Na^+, NH_4^+, Ag^+, H_3O^+) or divalent (Pb^{2+}, Ca^{2+}) cations (Jambor, 1999). When D is monovalent, TO_4 is dominantly SO_4, while when D is divalent, substitutions by PO_4 and AsO_4 commonly occurs (Jambor, 1999). The progression of replacement in the TO_4 site determines the change of classification from alunite group to beudantite, plumbogummite and dussertite groups (Scott, 1987; Bayliss et al., 2010). When TO_4 is $(SO_4)(PO_4)$ or $(SO_4)(AsO_4)$, the mineral is classified as one of the beudantite group (Palache et al., 1951; Jambor, 1999; Bayliss et al., 2010). When TO_4 is PO_4, the mineral belongs to the plumbogummite group, while when TO_4 is AsO_4, the mineral belongs to the dussertite group (Scott, 1987, Bayliss et al., 2010). The four groups, alunite, beudantite, plumbogummite and dussertite, are collectively called as the alunite supergroup (Bayliss et al., 2010).

Alunite is commonly found in acid-sulfate alteration zones associated with high-sulfidation epithermal deposits (e.g. Rye et al., 1991; Arribas et al., 1995a; Deyell et al., 2005; Chang et al., 2011). Hedenquist and Arribas (2022) summarized different sources of fluids that cause acid-sulfate alteration in a porphyry-type hydrothermal system. It includes quartz and alunite formed from fluids that condensed hypogene magmatic vapor into meteoric water and in steam-heated acid-sulfate environment caused by the condensation of CO_2 and H_2S-bearing fluids into meteoric water (Hedenquist and Arribas, 2022). Alunite also forms as a weathering product of sulfides in atmospheric environments (Ohmoto and Rye, 1979; Hayba et al., 1986; Hedenquist and Arribas, 2022). Alunite was also reported to have precipitated from Al-rich acidic fluids in the lacustrine environment (e.g. Long et al., 1992; Benison et al., 2007; Chambefort and Moritz, 2014; Sahlström et al., 2018; Sahlström et al., 2020). Terrestrial alunite-jarosite has also been used as analogs for the study of Martian jarosite (Papike et al., 2006). Recently, alunite was also discovered in Mars using images and visible/shortwave infrared spectra (Ehlmann et al., 2016). Studies on the effects of physical and chemical conditions on alunite formation can help us further our knowledge, not only of ore deposit formation, but of other planets, as well.

Several studies have been previously conducted to determine what factors affect the substitutions in the different sites of an alunite crystal lattice (e.g. Hemley et al., 1969; Hladky and Slansky, 1981; Stoffregen and Cygan, 1990; Deyell, 2001; Hedenquist et al., 2017). The most accepted explanation is based on the experimental work of Stoffregen and Cygan (1990) that reported the decrease of the equilibrium constant of the reaction (1) as the temperature decreases.

$$KAl_3(SO_4)_2(OH)_6 + Na^+ \leftrightarrow NaAl_3(SO_4)_2(OH)_6 + K^+ \quad (1)$$

This relationship indicates that the process of substitution of Na into K site in alunite is endothermic, thus, an increase in temperature would move the reaction towards the formation of natroalunite [$NaAl_3(SO_4)_2(OH)_6$]. They noted, however, that their experimental conditions may have led to an overestimation of the distribution coefficient (K_D, defined as the molar ratio of Na to K in the solid over that in the solution), and uncertainties in their mixing parameters are significant at temperatures below 250 °C.

Hemley et al. (1969) conducted experimental and computational approaches to determine the stability field of alunite from 200 to 380 °C. They mentioned that the rare occurrence of sodic alunites indicates a narrower stability field relative to the potassic alunite phase and that high Na to K ratio is required in the aqueous phase. Hladky and Slansky (1981) calculated the required K and Na activity ratios to form natroalunite at common temperature and pressure. They indicated that the concentration ratio in natural waters (White et al., 1963) is 1400 times less than the required ratio for natroalunite to precipitate. Deyell and Dipple (2005) calculated the concentration ratios of fluids required to form varying alunite-natroalunite compositions at 100 °C to 300 °C, pH 3, 0.2 M chlorinity and 0.01 M total sulfate, using the experimental parameters determined by Stoffregen and Cygan (1990). Their results indicated that to form Na-rich alunite (X_{Na} greater than 0.5) at 200 °C to 250 °C in an acidic environment, the K/Na molar concentration ratio of the fluids should be less than 10^{-2} order of magnitude. From reviewing different data sets of fluid chemistry of volcanic discharges and fluid inclusions in ore and gangue minerals, we found that fluids with K/Na ratios lower than 10^{-2} are rare (e.g. White et al., 1963; Kouzmanov et al., 2010; Audétat, 2019). However, the presence of Na-rich alunites has been well-documented in the literatures (e.g., Moss, 1958; Parker, 1962; Scott, 1992; Stoffregen and Alpers, 1992). Sodic alunites were reported to occur with pyrophyllite in the metamorphic rocks of Bushmanland, South Africa (Wise, 1975; Schoch et al., 1989). Diagenetic non-hydrothermal natroalunite was reported in bedded sedimentary rocks in Ras Sudar Sinai (Goldberry, 1980). Sodic alunites have also been documented in different hydrothermal systems associated with various high-sulfidation epithermal deposits (e.g., Lerouge et al., 2006; Voudouris, 2011; Hedenquist et al., 2017; Corral et al., 2016; Sahlström et al., 2018; Georgieva et al., 2020), commonly occurring with its K-rich counterpart. Currently, we have no fluid chemistry data that will allow the direct comparison of the mineral chemistry of alunite with K/Na ratios in aqueous solutions. The calculated K/Na ratios required to form Na-rich alunite are not attained by measured composition of different hydrothermal and geothermal fluids (e.g. White et al., 1963; Giggenbach, 1997; Deyell and Dipple, 2005; Kouzmanov et al., 2010). This may either mean that the available chemistry data of hydrothermal fluid do not represent hydrothermal solutions from which natroalunite was formed, or that the calculations using the current thermodynamic parameters are not enough to describe the complexity of the interplay of factors that affect the formation of alunite.

In this contribution, we present petrography, mineral chemistry and sulfur isotopic data on alunites from the Mankayan District, Philippines. Alunite is associated with quartz and pyrite in the ~ 2 km long lithocap in the Mankayan District (Arribas et al., 1995b; Chang et al., 2011; Hedenquist et al., 2017; Manalo et al., 2018, 2020). A quartz-alunite-pyrite assemblage characterizes the most extensive alteration zone in the district, and it surrounds the enargite-gold and quartz-pyrite-gold (QPG) veins. Previous studies have documented that the alunites in the Mankayan District formed at different ages (Arribas et al., 1995b; Manalo et al., 2020). In this paper, we further explore how the mineral chemistry and sulfur isotopic signature of these alunites vary. This contribution aims to identify the implications of these chemical and isotopic heterogeneities to the ore-forming conditions and fluid characteristics of the different mineralization events in the Mankayan District.

2. Geology and mineralization

The Mankayan District is located in the northern part of Luzon Island, along with other several porphyry copper–gold and epithermal gold deposits in the neighboring Baguio and Kalinga Mineral Districts (Fig. 1). The Mankayan District is underlain by a Cretaceous to Eocene metavolcanic basement called the Lepanto Metavolcanics (Garcia and Bongolan, 1989). The basement is unconformably overlain by Neogene volcaniclastic sequences of the Apaoan and Balili Volcaniclastics (Garcia and Bongolan, 1989). The basement rocks are intruded by the Middle Miocene Bagon Intrusives. Plio-Pleistocene magmatism was recorded by the porphyritic domes and pyroclastic deposits of the Imbanguila Dacite and Bato Dacite (Garcia and Bongolan, 1989). The Mankayan District is being traversed by several northwest-trending steeply-dipping faults, which controlled the epithermal gold mineralization in the Lepanto Main Enargite orebody and the Northwest quartz-pyrite-gold deposit (Fig. 1; Garcia and Bongolan, 1989; Subang, 2017).

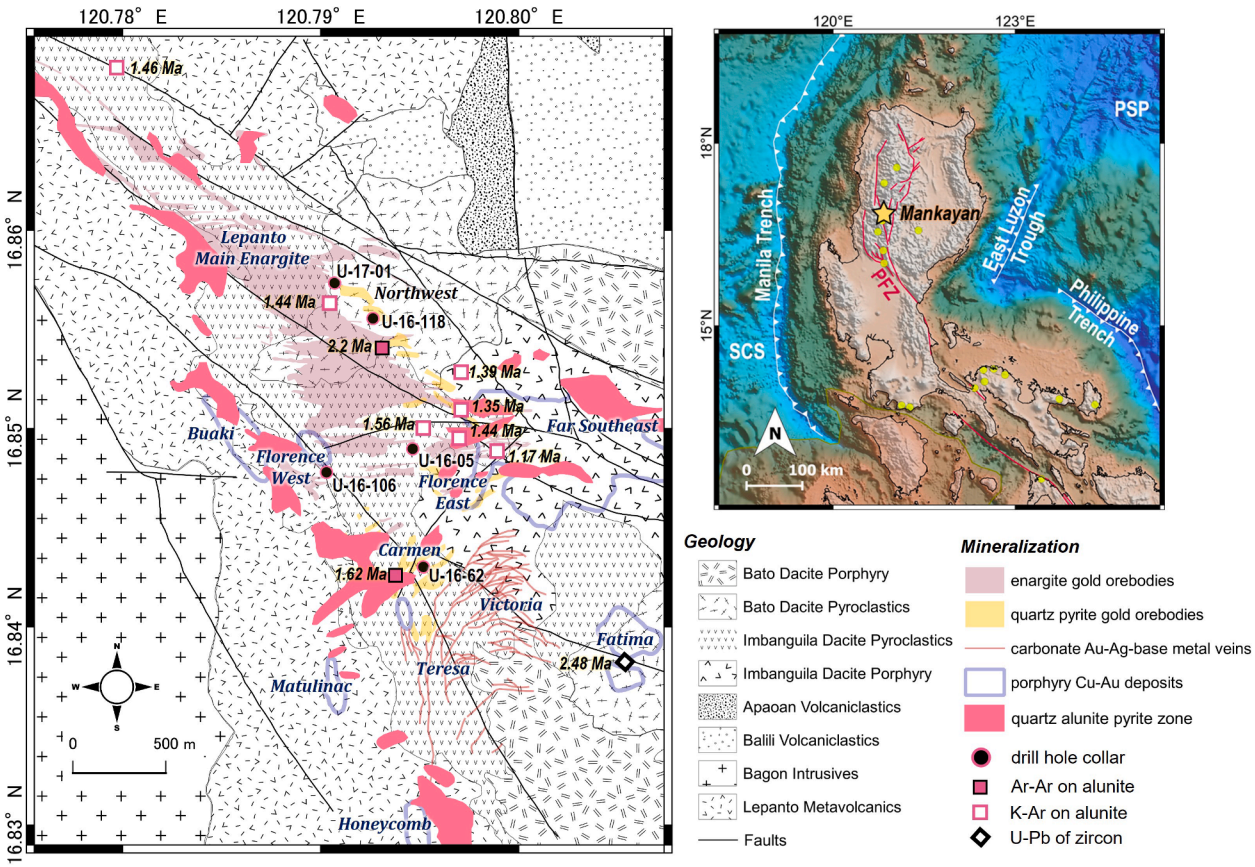

Fig. 1. Quartz-alunite-pyrite alteration map of the Mankayan District with plotted alunite ages reported by previous works (Arribas et al., 1995b; Cooke et al., 2004; Manalo et al., 2018, 2020). Inset shows the location of the Mankayan District in northern Luzon, Philippines. Topography and bathymetry were from Amante and Eakins (2009). Green dots show the location of other hydrothermal ore deposits from Jimenez et al., 2002. Abbreviations: SCS – South China Sea; PSP – Philippine Sea Plate; PFZ – Philippine Fault Zone. (For interpretation of the references to colour in this figure legend, the reader is referred to the web version of this article.)

Four types of mineralization have been recognized in Mankayan (Garcia and Bongolan, 1989; Imai, 2000; Subang, 2017; Manalo et al., 2018). These include several porphyry-type deposits that vary in age and depths (Sillitoe and Angeles, 1985; Arribas et al., 1995b; Cooke et al., 2004). The depths of the tops of the porphyry-type deposits increases from west to east, leading Subang (2017) to hypothesize an eastward younging trend for the generation of the porphyry deposits. The oldest porphyry-type deposits are probably the surface-exposed Buaki and Palidan deposits (Subang, 2017). Younger porphyry-type deposits include the Guinaoang and Bulalacao (now renamed as Fatima) deposits, which were formed in 3.5 ± 0.9 Ma (Sillitoe and Angeles, 1985) and 2.48 ± 0.42 Ma (Cooke et al., 2004), respectively. The youngest mineralization event occurred at 1.45 ± 0.04 Ma forming the world-class Far Southeast porphyry deposit (Arribas et al., 1995b).

In the southern part of the Mankayan District lies the Victoria and Teresa deposits. These deposits are both characterized by carbonate-base metal-gold-silver quartz veins (Claveria, 2001; Sajona et al., 2002). The north–south trending Teresa veins were formed at 2.22 ± 0.05 Ma (Chang et al., 2011), while the northeast-trending Victoria veins were formed from 1.31 ± 0.02 (Sakakibara et al., 2001) to 1.14 ± 0.02 Ma (Hedenquist et al., 2001).

The mineralization in the northern portion of the Mankayan District is dominated by the Lepanto Main Enargite orebody (Fig. 1; Garcia and Bongolan, 1989). K-Ar ages on alunite proximal to the orebody range from 1.56 ± 0.29 Ma to 1.17 ± 0.16 Ma (Arribas et al., 1995b). Recent exploration delineated other enargite orebodies in Carmen, Florence East and Florence West areas. Further south of the Mankayan District, presumably older enargite orebodies occur on top of the Guinaoang deposit.

The fourth style of mineralization in Mankayan has been first described by Garcia and Bongolan (1989) as post-enargite low copper, high-gold epithermal veins. This type of veins was further explored in 2015 and collectively called as the quartz-pyrite-gold (QPG) veins. The QPG veins have been delineated in the Northwest, Carmen, Florence East and Florence West areas (Fig. 1). A radiometric $^{39}Ar/^{40}Ar$ age on alunite from the Northwest QPG deposit is 2.2 ± 0.1 Ma (Manalo et al., 2018), while that from the Carmen QPG deposit is 1.62 ± 0.04 Ma (Manalo et al., 2020).

3. Materials and methods

Polished thin sections of alunite-bearing veins and altered host rocks of the Northwest, Carmen, Florence West and Florence East areas were prepared. Transmitted and reflected light petrography were conducted using a Nikon Eclipse LV100N POL polarizing microscope. The presence of alunite was confirmed using X-ray diffraction (XRD) spectroscopy of powdered rock samples. XRD analysis was conducted using a Rigaku Multiflex X-ray diffractometer with Cu-Kα radiation generated at 30 kV and 16 mA. The samples were scanned from 2° to 60° 2θ with a scan speed of 2°/min and a step width of 0.010°.

Chemical composition of alunite crystals was determined on polished thin sections using a JEOL JXA-8230 electron probe microanalyzer (EPMA) operated in the wavelength-dispersion mode at 15 kV acceleration voltage, 10nA beam current and 15 μm beam diameter. The operating conditions were adapted from Deyell et al. (2005). The analyzed elements include K, Fe, Al, Na, P, Ba, S, Pb and Ca, and were standardized against $KAlSi_3O_8$, Fe_2O_3, Al_2O_3, $NaAlSi_3O_8$, CeP_5O_{14}, $BaSO_4$, $BaSO_4$, PbS and $CaSiO_3$, respectively. The average detection

limits are 100 ppm for K_2O, 250 ppm for FeO, 260 ppm for Al_2O_3, 260 ppm for Na_2O, 220 ppm for P_2O_5, 520 ppm for BaO, 300 ppm for SO_3 and 110 ppm for CaO.

Sulfur isotopic ratios of alunite and coexisting pyrite were determined. Alunite and pyrite crystals were carefully separated by hand-picking under a binocular microscope. Individual crystals of pyrite are usually larger than 150 μm and were easy to separate. Alunite crystals, on the other hand, occur as finer crystals and are intricately associated with quartz and kaolinite or dickite.

Twenty milligrams of pyrite were decomposed using 20 mL 16 M HNO_3 and 2 mL Br_2 at 90 °C. After overnight evaporation of the solution, the residue was dissolved in 10 mL 6 M HCl. The acidified solution was diluted to 100 mL and passed through a cation exchange column. Ten milliliters of 10 % $BaCl_2$ solution was added to the 300 mL eluent to precipitate $BaSO_4$.

Alunite-rich fragments were separated from lightly crushed rock

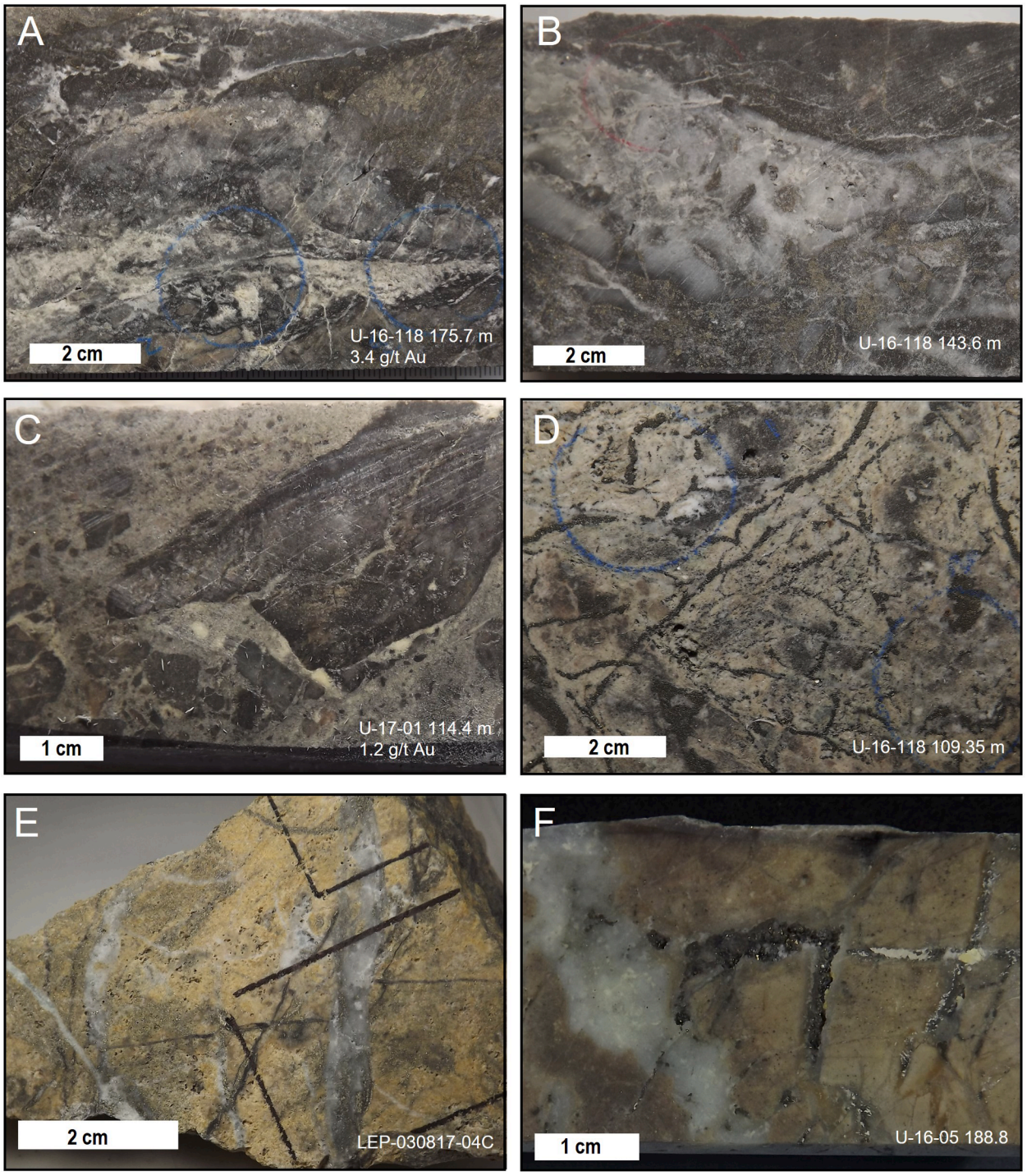

Fig. 2. Photos of representative drill core samples from Northwest (A to D), Carmen (E), and Florence East (F). A. Alunite occurs as creamy white fine-grained crystals filling in a fracture (drillhole U-16–118 175.7 m). B. Alunite occurs as creamy white patches within the quartz vein (drill hole U-16–118 143.6 m). C. Alunite occurs as creamy white patches within the matrix surrounding the angular clasts (drillhole U-17–01 114.4 m). D. Alunite occurs as pervasive alteration of the rock (drillhole U-16–118 109.35 m). Sulfide stringers are abundant. E. Alunite occurs within the quartz veins and filling-in vugs in the rock (LEP-030817-04C from UG L900). F. Alunite occurs as fine-grained creamy white crystals that filled in the fractures of the rock (drillhole U-16–05 185.8 m).

samples by hand picking under a binocular microscope. Separates containing approximately 250 mg equivalent of alunite were dissolved in 200 mL of freshly prepared 0.5 M NaOH solution at 80 °C for 12 h. Undissolved impurities, such as quartz and clay minerals, were filtered out. The filtered solution passed through a cation exchange column. The eluent was then acidified by 10 mL 6 M HCl to prevent the precipitation of $Al(OH)_3$. Ten milliliters of 10 % $BaCl_2$ solution was added to the 300 mL eluent to precipitate $BaSO_4$.

The precipitated $BaSO_4$ was collected using a syringe with membrane filter. The $BaSO_4$ (0.4 to 0.5 mg) recovered was packed with V_2O_5 powder in a tin foil. The packed samples were loaded into the automatic sampler attached to a Thermo Fisher Flash 2000 Elemental Analyzer, where the samples were combusted in a quartz tube at 1020 °C. The combustion yielded SO_2 gas and was separated by gas chromatography. Isotopic ratios were measured using a Thermo Fisher Scientific Delta V Advantage isotope ratio monitoring mass spectrometer. Calibration curves were constructed using IAEA NBS-127 ($\delta^{34}S_{CDT} = +20.30$ ‰), IAEA SO-6 ($\delta^{34}S_{CDT} = -34.10$ ‰), and IAEA SO-5 ($\delta^{34}S_{CDT} = +0.50$ ‰) (Halas and Szaran, 2001). Sulfur isotope ratio is presented relative to the $^{34}S/^{32}S$ value of troilite of the Canyon Diablo meteorite ($\delta^{34}S_{CDT}$ in ‰). The analytical uncertainty is ± 0.2 ‰.

4. Results

4.1. Alunite occurrence

In hand samples, alunite occurs as a fine-grained creamy white mineral, commonly found within veins and fracture-fills (Fig. 2A, 2B). It also occurs as white patches of cement surrounding clasts of lithic fragments (Fig. 2C). In some samples, alunite occurs as pervasive alteration of the volcanic host rocks (Fig. 2D, 2E). Alunite was also found overprinting volcanic rocks that host porphyry-type veins (Fig. 2E, Manalo et al., 2020). Sulfides closely associated with alunite include pyrite and enargite that occur as dissemination in the host rock (Fig. 2B), as stringers (Fig. 2D) or as open-space fillings (Fig. 2F).

Under the microscope, alunite crystals vary in size. (Fig. 3A to 3F). Anhedral crystals of fine-grained alunite occur as aggregates (Fig. 3A) filling vugs or intergrown with anhedral quartz (Fig. 3B). Coarser alunite usually occurs as tabular crystals intergrown with subhedral quartz and pyrite in veins (Fig. 3C, 3D). The crystal size of sulfide minerals relative to the size of alunite crystals also vary from one sample to another. In some samples, coarse anhedral pyrite crystals are surrounded by fine crystals of tabular alunite (Fig. 3E, 3F). The crystal size of alunite can vary greatly within a single vein (Fig. 3G). Some samples from Carmen contain anhedral anhydrite crystals that have been replaced by fine-grained alunite (Fig. 3H).

4.2. Mineral chemistry

4.2.1. Compositional mapping

Secondary electron images (SEI) show intergrown tabular alunite crystals (Fig. 4A). Compositional heterogeneity within a single crystal is evident from the backscattered electron images (BSE; Fig. 4B). Elemental mapping of alunite crystals indicates that the S and Al contents are mostly constant throughout (Fig. 4C, 4D). The compositional zones are mainly caused by the variations in the Na and K contents. Some alunite crystals have a high-K core, surrounded by low to intermediate-K zones (Fig. 4E). Most of the alunite crystals with relatively low K content have high Na content (Fig. 4F). Alunite crystals with homogeneous K or Na contents are also present. Compositionally homogeneous and heterogeneous alunite crystals are commonly found intergrown with each other (Fig. 4E, 4F). This K-Na type of alunites is abundant in Northwest, Carmen, Florence East and Florence West.

The Ca content of some alunite crystals is slightly elevated, but its occurrence is not as abundant as those of K-Na alunites (Fig. 5A to 5E). Calcium-bearing alunites were found in 830 m to 860 m elevation in Northwest, in 900 m elevation level in Carmen and 1131 m elevation in Florence West. These alunite crystals coexist with anhedral quartz and anhedral pyrite (Fig. 5A). These Ca-bearing alunites are homogeneous in S and Al (Fig. 5B, 5C). The compositional variations observed in BSE images are due to variable K, Na and Ca contents (Fig. 5D to 5E). Thin K-rich zones are randomly distributed among the alunite crystals (Fig. 5D).

Few crystals of aluminum-phosphate-sulfate (APS) minerals were also observed in the Northwest and Florence West areas. The APS minerals appear very bright in BSE images (Fig. 6A). The APS minerals are tightly intergrown with K-Na alunite crystals, often showing anhedral morphology. Anhedral to subhedral pyrite and quartz commonly coexist with the APS mineral crystals. The elemental maps of these crystals show variable S contents. In zones where the S content is low, the P content is high (Fig. 6B, 6C). The relative concentrations of K, Na and Ca also vary within the crystals (Fig. 6D to 6F). The high Ca content corresponds to the low K and low Na contents in the elemental maps. The Al content, on the other hand, is constant within a crystal and among different crystals. Some APS minerals occur within the core of anhedral alunite crystals intergrown with quartz (Fig. 7A, 7B). The high P content corresponds to low S content in the elemental maps (Fig. 7C, 7D). The surrounding alunite crystals have slight variations in K and Na (Fig. 7E, 7F). While the K and Na contents of the core of APS are very low, the amount of Ca is high (Fig. 7G). Small amounts of Ba were also detected within the core of APS (Fig. 7H).

From the elemental map analysis, we found that morphology and compositions of alunite group vary within a single crystal, as well as from one crystal to another. From the several analyzed samples, we found that the Al concentration remained constant. Sulfur was replaced by P in few alunite crystals. Tabular alunites in different localities are often characterized by either high K or high Na content. Alunite that contains significant Ca are commonly anhedral in shape. Regardless of composition, most alunites coexist with quartz and pyrite.

4.2.2. Point analysis

Point analyses of alunite crystals were conducted to quantitatively determine the composition of alunite crystals in different samples (Supplementary Data Table 1). The measured concentrations were recalculated assuming that the OH content is stoichiometric. The total recalculated number of atoms per formula unit (apfu) of SO_4 and PO_4 is 2 and that of Al is 3 apfu. The sum of K and Na is mostly 1 apfu, except for crystals that contain significant amount of Ca. In the analyses of over 1000 points, no significant Fe content was detected, indicating the absence of jarosite group in the samples.

A ternary plot of (Na + K)-(Sr + Ba + Pb)-Ca (Fig. 8) shows that most of the crystals analyzed from Mankayan District belong to the alunite-natroalunite group. The samples from the lower elevation level of the Northwest (U-16–118 186.3 and U-16–118 197.8) also contain APS minerals in addition to alunite – natroalunite (Fig. 8; Supplementary Data Table 1). One sample from Florence West (U-16–106 55.5) contains mostly alunite – natroalunite with a few Ca substitution. Another sample (U-16–106 67.5 m) only contains woodhouseite [$CaAl_3(SO_4)(PO_4)(OH)_6$], with no significant Na and K content. The woodhouseite crystals occur as tiny inclusions in quartz (Fig. 8; Supplementary Data Fig. 2).

Since the variation of the chemical composition of the alunite samples are mostly due to K, Na and Ca, we plotted the composition on ternary diagrams K-Na-Ca (Figs. 9 and 10). Six samples of the Northwest QPG deposit from different elevation were analyzed (Fig. 9). Compositions of most alunite crystals from the Northwest QPG deposit widely vary from K-rich to Na-rich. In the lower elevation levels (830 m to 860 m), a few Ca-rich alunite and APS minerals are present. The K content of alunite ranges from 0 to 0.98 apfu, with an average of 0.49 apfu. The K content of the other samples likewise varies widely, averaging mostly at the intermediate K-Na compositions. The average K content of the sample U-17–01 114.4 m is the lowest at 0.38 apfu.

The chemical compositions of alunite from the Carmen QPG deposit are variable between the K-rich and Na-rich end members, as well as the

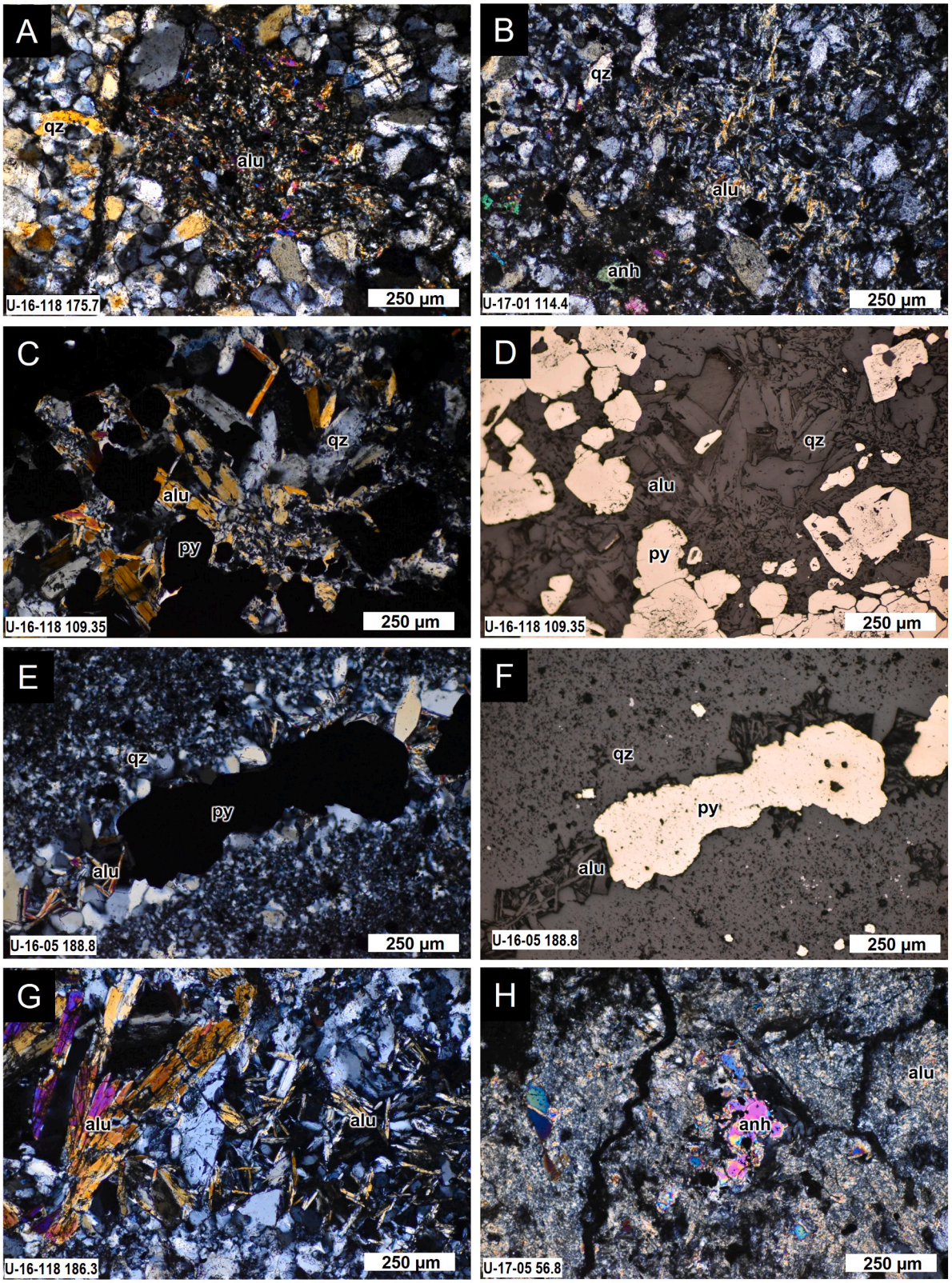

Fig. 3. Photomicrographs of alunite samples. A) Alunite occur as fine-grained anhedral open-space fillings. B) Alunite occurs as pervasive alteration of the host rock. C and D) Crossed polars transmitted light photomicrograph and reflected light photomicrograph showing subhedral to euhedral pyrite occurring with tabular alunite and quartz. E and F) Coarse pyrite and fine-grained tabular alunite occurring within a vein. G) Tabular and acicular alunite crystals occurring within the interstices of anhedral quartz. H) Anhydrite being replaced by fine-grained alunite. A, B, C, D, E and G: Northwest; F: Florence East; H: Carmen. Mineral abbreviations are from Whitney and Evans (2010).

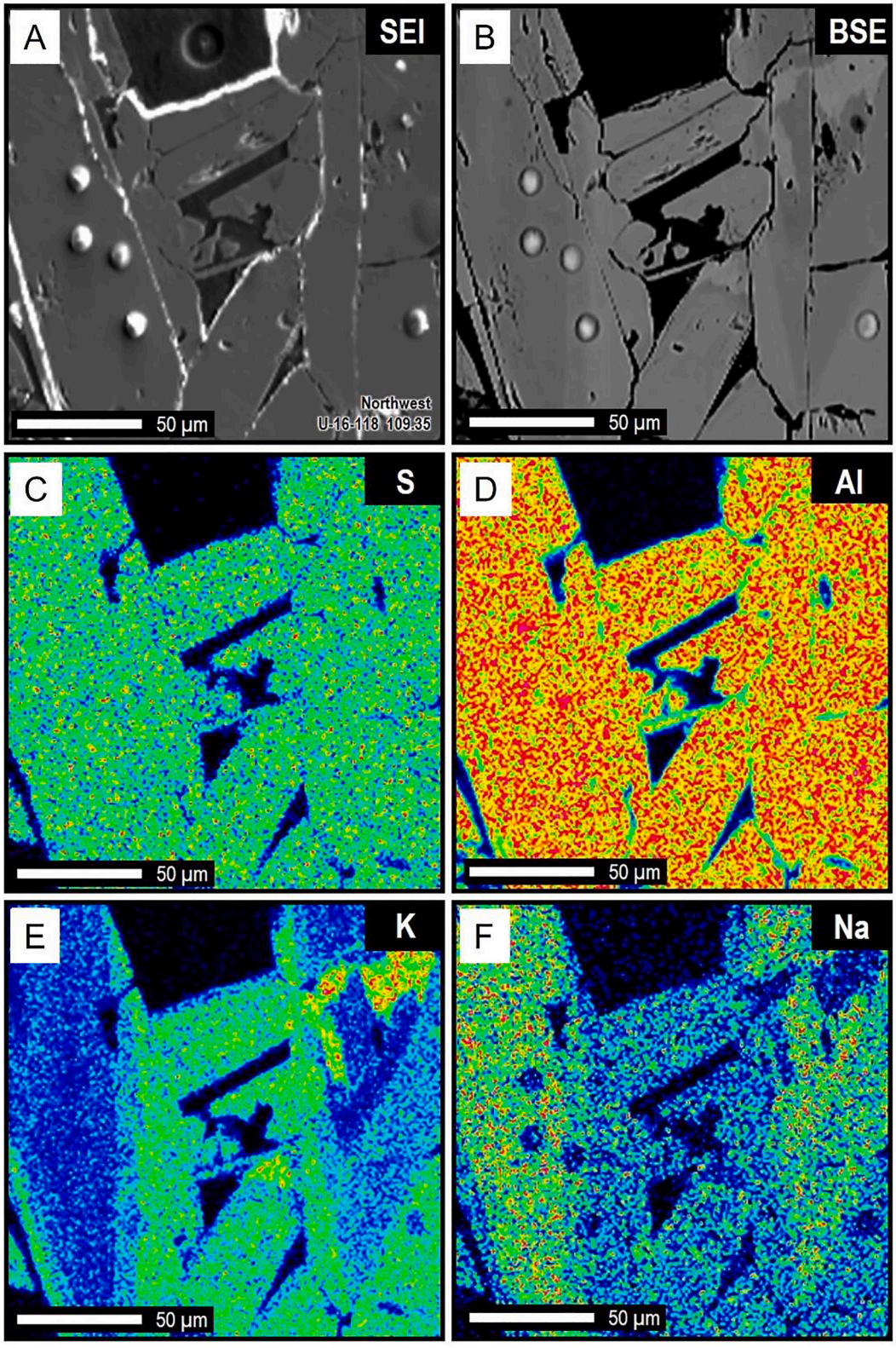

Fig. 4. Electron microscope images and elemental maps of alunite from the Northwest QPG veins (drillhole U-16–118 109.35 m). A) Secondary electron image of tabular alunite. The circular features are caused by beam damage during point analysis. B) Backscattered electron image of alunite showing light grey and dark grey bands within a crystal. C) Map of sulfur concentration in the alunite crystals shows that S content is constant throughout the crystals. D) Aluminum concentration map shows homogeneous distribution. E) Potassium concentration varies within an alunite crystal and among individual crystals. The relatively larger alunite crystal on the top right shows a high-K core (red), surrounded by a low-K zone (blue). F) Sodium concentration map shows that high-Na zones correspond to low-K zones. (For interpretation of the references to colour in this figure legend, the reader is referred to the web version of this article.)

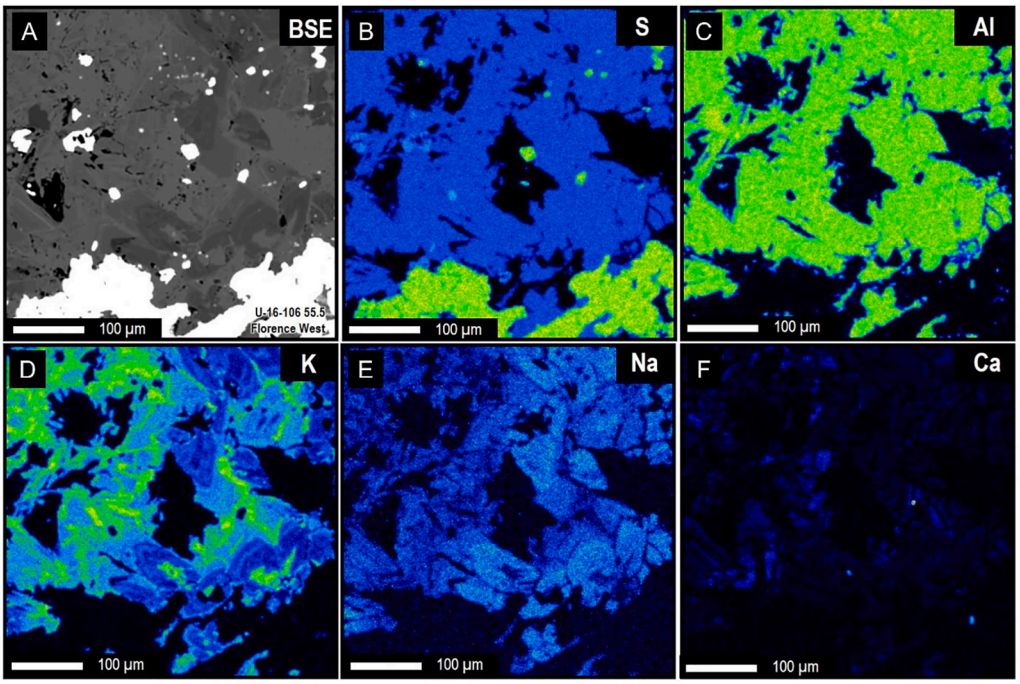

Fig. 5. Backscattered electron image (A) and elemental composition map (B – F) of alunite in U-16–106 55.5 m (Florence West). The crystals have uniform sulfur content, with no detectable phosphorous. Aluminum content is also the same throughout the area. The zonation in the backscattered image corresponds with the content of K and Ca.

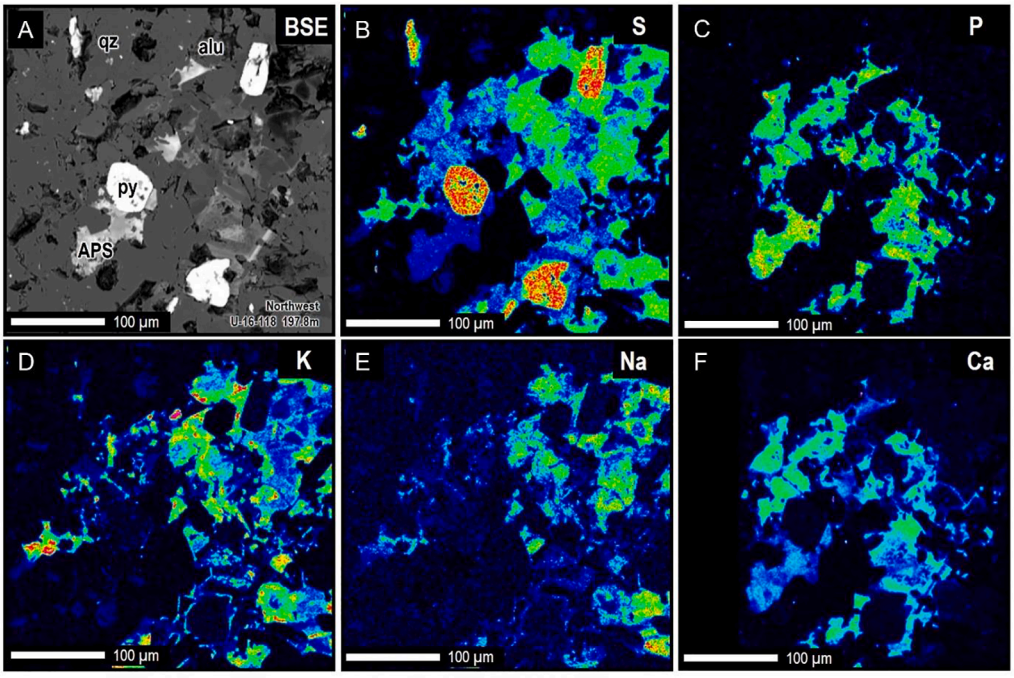

Fig. 6. Backscattered electron image (A) and elemental composition map (B – F) of alunite and APS minerals in U-16–118 197.8 m (Northwest) showing the variation of sulfur and phosphorous content in anhedral crystals. The K and Na content of the S-rich parts are variable with no clear zonation. Areas with high P content coincide with high concentrations of Ca and low concentrations of K and Na. Mineral abbreviations are from Whitney and Evans (2010): qz – quartz; alu – alunite; py – pyrite; APS – aluminum phosphate sulfate.

Ca content (Fig. 10). The K content varies from 0.27 to 0.92 apfu, with an average of 0.51 apfu. Significant Ca content of few crystals ranges from 0.12 to 0.29 apfu. Alunite crystals from Florence East, on the other hand, are mostly confined to the K-Na solid solution (Fig. 10). The K content of the alunite from underground (L900 m) sample (Lep-032017–09) ranges from 0.18 to 0.98 apfu, while that of the drillhole sample (U-16–05 172.3 m) ranges from 0.005 to 0.77 apfu. The average K content of both samples is 0.56 apfu. The compositions of alunite crystals from one sample in Florence West (U-16–106 55.5 m) are variable between the K-rich and Na-rich end members (Fig. 10). The K content of the alunite varies from 0.12 to 0.98 apfu, with an average of 0.42 apfu.

4.3. Sulfur isotopes

Most of the $\delta^{34}S$ of alunite analyzed in this study range from + 13 ‰

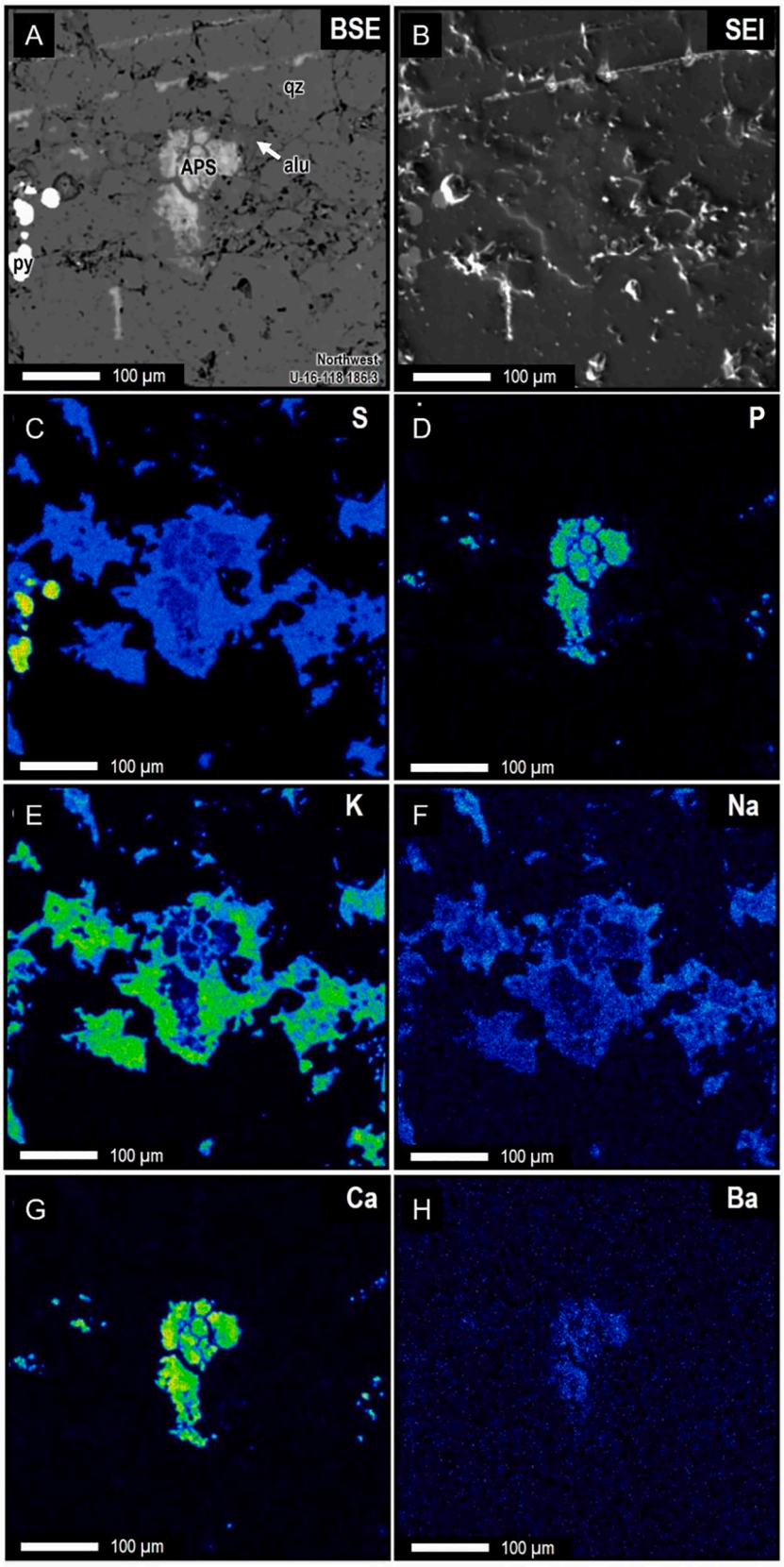

Fig. 7. Electron microscope images (A and B) and elemental maps (C – H) of alunite in U-16–118 186.3 m (Northwest) showing a core with high PO_4 and Ca content. The core also contains detectable amount of Ba. The core is surrounded by alunite rich in S and K. Mineral abbreviations are from Whitney and Evans (2010): qz – quartz; alu – alunite; py – pyrite; APS – aluminum phosphate sulfate.

Table 1
Sulfur isotopic data of alunite and pyrite from the Mankayan lithocap.

Sample ID	sulfide mineral	$\delta^{34}S_{CDT}$	sulfate mineral	$\delta^{34}S_{CDT}$	Isotopic Equilibrium Temperature (°C)	Homogenization Temperature of Fluid Inclusions in Quartz (°C)	Age
Carmen‡							
U-17–05 24.86	pyrite	+2.1	anhydrite	+14.1	455		
U-17–05 56.8	pyrite	−4.1	anhydrite	+24.5	192		
U-17–05 57.60	pyrite	−1.4	anhydrite	+22.6	235		
U-17–05 49.2	pyrite	−2.2	anhydrite	+24.3	210		
Lep-030817-04C	pyrite	−3.7	alunite	+22.9	197		
Lep-030817-04B						Range: 320 – 360 °C	
U-16–62 160.9			alunite	−3.9	supergene?		
U-16–62 168.57	pyrite	−4.2	alunite	+20.5	220		
U-16–62 185.2	pyrite	−2.2	alunite	+22.6	219		1.62 ± 0.04 Ma ($^{40}Ar/^{39}Ar$)
U-16–62 187.3						Range: 293 – 360 °C	
Florence West							
U-16–106 55.5	pyrite	−1.5	alunite	+19.6	274		
U-16–106 67.5	pyrite	−5.8	woodhouseite	−6.5	supergene?		
U-16–106 59.0	pyrite	−5.6	alunite	−3.6	supergene?		
Florence East							
LEP-032017–09			alunite	+20.1			
U-16–05 188.8	pyrite	−3.8	alunite	+13.2	364	Mode: 250 – 270 °C Range: 229 – 271 °C	
U-16–05 172.3	enargite	−3.4	alunite	+23.3	226		
Northwest‡‡							
U-17–01 114.4	pyrite	−5.4	alunite	+19.8	214		
U-16–118 109.35	pyrite	−2.8	alunite	+22.8	225		
U-16–118 117.5	pyrite	−1.8	alunite	+15.5	382		
U-16–118 128.65	pyrite	−2.8	alunite	+18.0	300		
U-16–118 138.8	pyrite	−1.2	alunite	+16.7	366		
U-16–118 171.8	pyrite	−1.0	alunite	+20.8	281		
U-16–118 175.7	pyrite	−1.8	alunite	+20.6	271		
U-16–118 179.9	pyrite	−3.3	alunite	+21.6	234	Mode: 220 – 230 °C Range: 204 – 348 °C	
U-16–118 186.3	pyrite	−3.8	alunite	+24.2	197	Range: 244 – 291 °C	
U-16–118 197.8	pyrite	−1.0	alunite	+21.1	277		
U-16–118 143.6			alunite				2.2 ± 0.1 Ma ($^{40}Ar/^{39}Ar$)
Lepanto Main Orebody*							
U89-34–630	pyrite	−1.8	alunite	+23.4	218		1.56 ± 0.29 Ma (K-Ar)
U91-42–156	pyrite	−0.5	alunite	+24.6	224		1.17 ± 0.16 Ma (K-Ar)

‡ Age data of alunite is from Manalo et al. (2020).
‡‡ Data of samples in italics are from Manalo et al. (2018).
* Sulfur isotopes and age data are from Hedenquist et al. (2017) and Arribas et al. (1995a), respectively.

to + 24 ‰ (Fig. 11; Table 1). The $\delta^{34}S$ of pyrite and enargite coexisting with alunite range from −5.4 ‰ to −1.0 ‰, which are typical isotopic signature of sulfides with sulfur isotopic fractionation from an H_2S-rich fluid exsolved from magma (Sakai and Matsubaya, 1977; Ohmoto and Rye, 1979; Bethke et al., 2005). The $\delta^{34}S$ of one alunite sample from Carmen (U-16–62 160.9 m; Table 1) and two alunite samples from the Florence West area (U-16–106 67.5 and U-16–106 59.0 m) are negative (-3.9 ‰, −6.5 ‰ and −3.6 ‰, respectively). The $\delta^{34}S$ of the alunite and APS mineral from Florence West are nearly equal to those of the coexisting pyrite (Table 1). Manalo et al. (2018) also reported the $\delta^{34}S$ of one alunite sample from Northwest (drillhole U-17–01 111.2) as −2.0 ‰, while that of its coexisting pyrite is −3.4 ‰. This type of alunite typically indicates supergene formation (Rye, 2005). Due to the very fine crystal size of these alunite crystals and their intricate intergrowth with enargite and pyrite, it may be argued that the sulfur isotope results of these samples may have suffered from the influence of micrometric sulfide impurities. Watanabe and Hedenquist (2001) reported that their analysis of alunite using NaOH dissolution were unaffected by trace sulfide impurities, but they found APS cores are resistant to NaOH dissolution. It is also possible that the negative $\delta^{34}S$ may not be representative of the sulfur isotopic value of the APS minerals but may be attributed to partial replacement of supergene alunite.

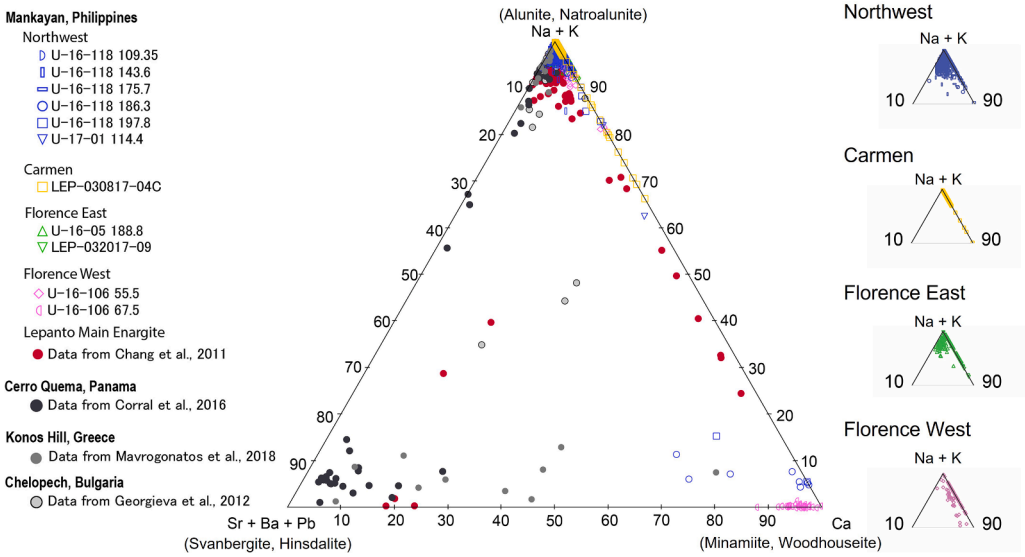

Fig. 8. Ternary plot of Na + K, Sr + Ba + Pb and Ca showing the variation in the compositions of alunite – APS minerals in Mankayan District and other lithocaps. Most of the crystals included in this study are alunite – natroalunite. The deeper samples from Northwest and samples from Florence West contain Ca-rich natroalunite (previously known as minamiite) or woodhouseite.

The sulfur isotopic signatures of anhydrite – pyrite veins in Carmen were also analyzed (Table 1). Earlier paragenetic studies indicate that the anhydrite vein formation postdated the alunite crystallization (Manalo et al., 2020). The $\delta^{34}S$ of anhydrite range from + 14.1 to + 24.5 ‰, while those of the associated pyrite crystals range from −4.1 to + 2.1 ‰.

The $\delta^{34}S$ of alunite and anhydrite in Northwest, Carmen, Florence East and Florence West areas mostly range between + 20 and + 25 ‰ (Table 1). The $\delta^{34}S$ of two alunite samples from Northwest ($\delta^{34}S$ = +15.5 to + 16.7 ‰), one alunite sample from Florence East ($\delta^{34}S$ = +13.2 ‰) and one anhydrite sample from Carmen ($\delta^{34}S$ = +14.1 ‰) are lower. The lower $\delta^{34}S$ of sulfate (+13 to + 17 ‰) may indicate lesser degree of fractionation between the sulfide and sulfate, which are common at higher temperatures (Ohmoto and Goldhaber, 1997). The $\delta^{34}S$ of coexisting sulfide minerals in the four areas narrowly range from −5.8 to −1.0 ‰, except for one positive $\delta^{34}S$ of pyrite in Carmen ($\delta^{34}S$ = +2.1 ‰). Similar $\delta^{34}S$ of anhydrite and $\delta^{34}S$ of coexisting sulfides that indicated small isotopic fractionation were also reported from the FSE deposit (Imai, 2000).

The temperature of formation based on isotopic equilibrium was calculated from the hypogene alunite-pyrite pairs using equation (2) and equation (3) for temperatures greater than 400 °C and less than 350 °C, respectively (Ohmoto and Rye, 1979).

$$T = \frac{2.76 \times 10^3}{(\Delta \pm 1)^{1/2}} \quad (2)$$

$$T = \frac{2.16 \times 10^3}{(\Delta - 6 \pm 0.5)^{1/2}} \quad (3)$$

For alunite – enargite pairs, we used the sulfur isotopic fractionation factors of aqueous sulfate and sphalerite, since enargite is expected to behave like sphalerite due to their similar structure (Hedenquist et al., 2017), leading to equation (4).

$$T = \left(\frac{5.16 \times 10^6}{(\Delta - 6)}\right)^{1/2} \quad (4)$$

For anhydrite – pyrite pairs, we used equation (5) after Ohmoto and Lasaga (1982) and Ohmoto and Rye (1979).

$$T = \left(\frac{6.063 \times 10^6}{(\Delta - 0.56)}\right)^{1/2} \quad (5)$$

The formation temperatures calculated from alunite-pyrite, alunite-enargite, and anhydrite-pyrite pairs vary greatly across different localities. In Carmen, isotopic equilibrium temperatures below 200 °C were calculated from one alunite-pyrite pair (197 °C) and anhydrite-pyrite pair (192 °C). Moderate temperatures (210–230 °C) were calculated from both alunite-pyrite and anhydrite-pyrite pairs. The highest temperature (455 °C) was calculated from the anhydrite-pyrite pair with the lowest $\delta^{34}S$ of anhydrite and the only positive $\delta^{34}S$ of pyrite (Table 1). The alunite-pyrite pair from Florence West yielded an isotopic equilibrium temperature of 274 °C, which is a little higher than those of the alunite-pyrite pairs from Carmen. In Florence East, the alunite-pyrite pair yielded a calculated isotopic equilibrium temperature of 364 °C. This is significantly higher than the isotopic equilibrium temperature of an alunite-enargite pair (226 °C) that was taken about 15 m away.

5. Discussion

5.1. Alunite heterogeneity in the lithocap at Mankayan

5.1.1. Sulfur isotopes

The range of the $\delta^{34}S$ of alunite (+13 to + 24 ‰) and sulfides (-5.4 ‰ to + 2.1 ‰) are typical signatures of alunite and sulfides that formed from hydrothermal processes (Field, 1966; Rye et al., 1992; Rye, 2005; Hutchison et al., 2020). The hypogene nature of alunite is also consistent with the coarse crystal size, tabular habit and intricate association with hydrothermal quartz, enargite and pyrite (Rye, 2005; Manalo et al., 2018). The $\delta^{34}S$ of hypogene alunite are typically higher than those of the coexisting sulfides because ^{34}S preferentially fractionates to the sulfate phase (e.g., Hutchison et al., 2020).

For Northwest and Carmen, significant numbers of isotopic ratios of sulfide and sulfate minerals have been determined, which allows us to examine the variations. The sulfur isotopic ratios of sulfide minerals range narrowly, indicating that H_2S is the dominant sulfur species (Sakai, 1968; Rye, 2005; Manalo et al., 2018). Furthermore, the bulk $\delta^{34}S$ can be calculated following the methods described by Field and Gustafson (1976). Manalo et al. (2018) already reported the bulk $\delta^{34}S$ in the Northwest area as + 5 ‰. It is similar to the bulk $\delta^{34}S$ of the Far Southeast porphyry Cu deposit (+6 ‰) reported independently by Imai

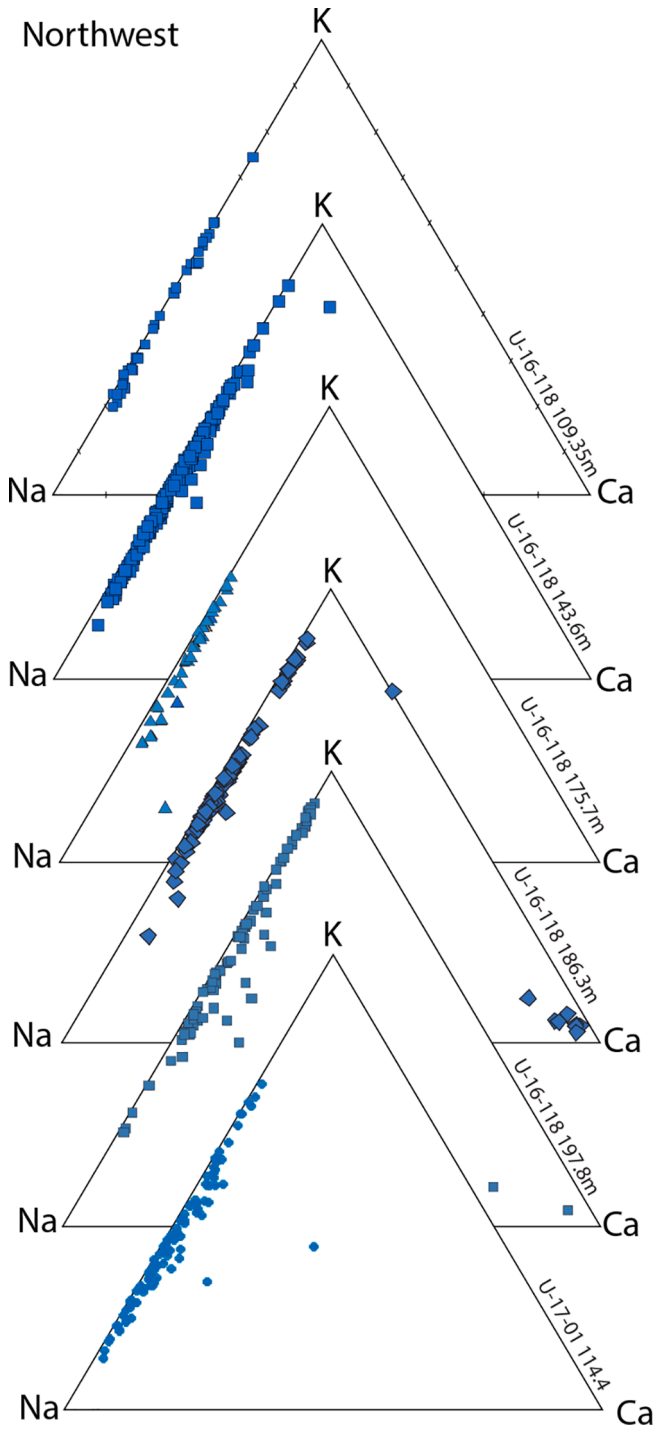

Fig. 9. Ternary diagrams showing the variations of K, Na and Ca contents of alunite in the samples from the different drill hole samples in the Northwest area. A widespread variation of composition along the Na-K substitution line is common. Significant Ca content is seen in deeper drillhole samples. The samples are arranged according to increasing depth from top to bottom.

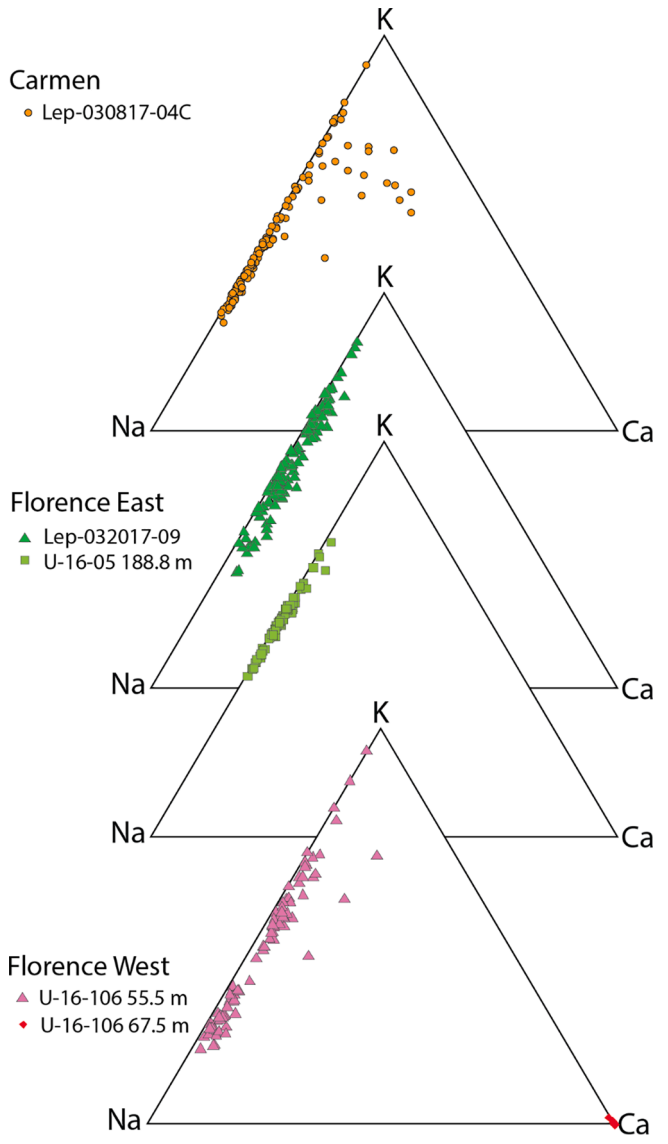

Fig. 10. Na-K-C ternary diagrams of alunite from Carmen, Florence East and Florence West. Composition varies widely along the K-Na substitution line. The alunite from Carmen and Florence West shows Ca substitution.

(2000) and Hedenquist et al. (2017). The bulk $\delta^{34}S$ for the Lepanto Main Enargite orebody was determined by Hedenquist et al. (2017) as + 2 ‰. In this study, we add the data for the anhydrite-pyrite and alunite-pyrite pairs from Carmen area and determined the bulk $\delta^{34}S$ for Carmen as + 6 ‰ (Fig. 12). From these data, we see that the bulk $\delta^{34}S$ of the different magmatic-hydrothermal systems in Mankayan are similar in value, despite the varying radiometric ages of alunite. In other lithocaps, Deyell et al. (2005) reported a bulk $\delta^{34}S$ of + 1 to + 3 ‰ for magmatic steam alunite in the Tambo high sulfidation deposit in Chile, while Corral et al. (2017) reported a bulk $\delta^{34}S$ of −0.5 ‰ for the Cerro Quema Au-Cu deposit in Panama.

Although the number of data is limited, we plotted the data of the alunite-pyrite pairs from Florence East and Florence West areas (Fig. 12). If the conditions of sulfur isotopic fractionation are the same for the samples from different areas, the alunite-pyrite and alunite-enargite pairs would plot along the same range as the other deposits, in the same way that the data from Far Southeast, Carmen and Northwest areas overlap each other. The data of the alunite-pyrite pair from Florence West (U-16–106 55.5) and the alunite-enargite pair from Florence East (U-16–05 172.3) are within the similar range as the alunite-pyrite pairs of Carmen and Northwest. However, the $\delta^{34}S$ of an alunite-pyrite pair of Florence East (U-16–05 188; +13.2 ‰, −3.8‰) are significantly out of trend. Furthermore, both the trendlines of the sulfates and sulfides in Florence East, drawn from an alunite-pyrite pair and an alunite-enargite pair, have positive slope, and both measured $\delta^{34}S$ of sulfides and sulfates are greater than the calculated bulk $\delta^{34}S$. This could not be physically possible since fractionation from a single source should lead to the enrichment of ^{34}S in the sulfate and depletion of ^{34}S in the

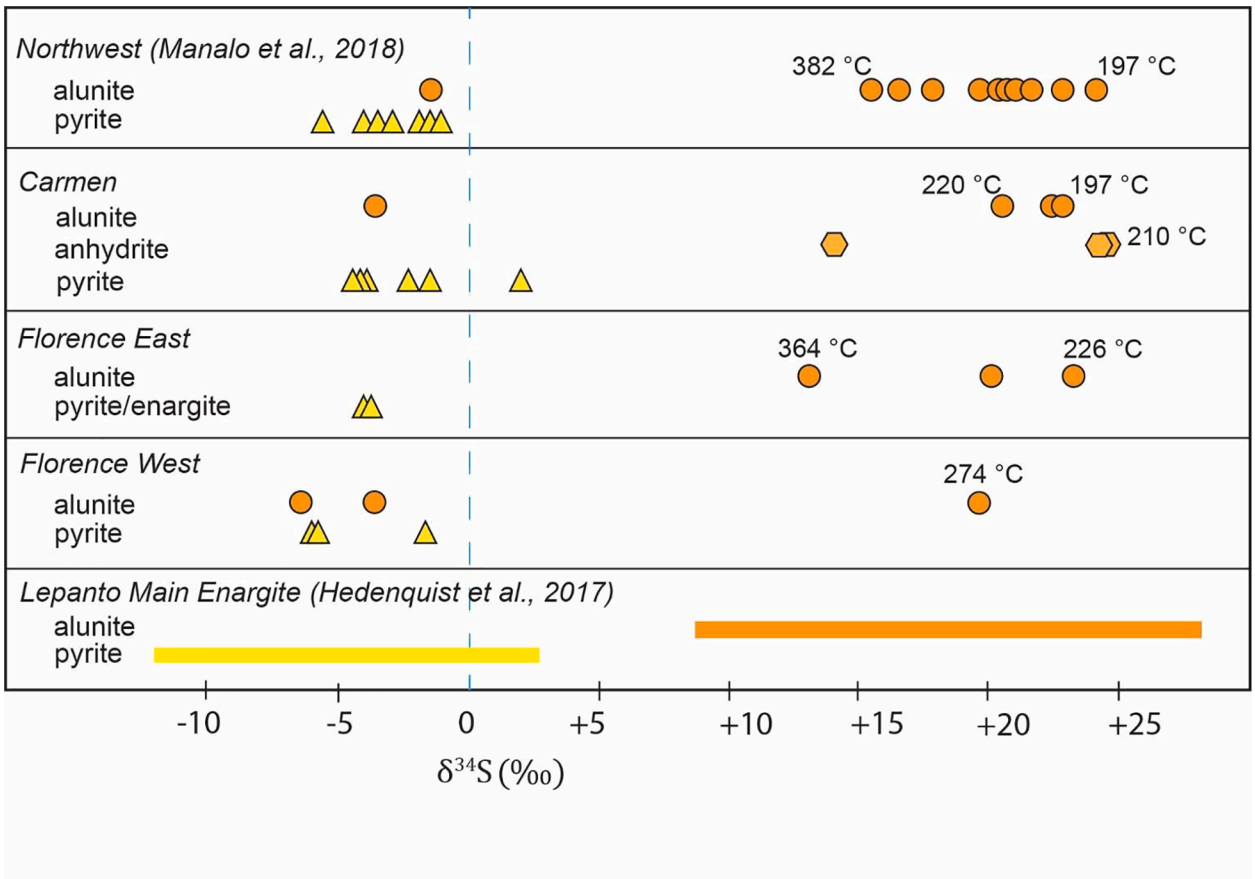

Fig. 11. Range of sulfur isotopic ratios ($\delta^{34}S$) of the sulfides and sulfates from the different deposits in the Mankayan District. The data from the Northwest QPG deposit were from Manalo et al. (2018) and those from the Lepanto Main Enargite orebody are from Hedenquist et al. (2017).

sulfides. This indicates that the alunite, pyrite and enargite from the Florence East were not in isotopic equilibrium. The trendline intersection for Florence East (Fig. 12) does not represent the true value of the bulk $\delta^{34}S$ of the hydrothermal fluid. More data is necessary to get a proper estimate of the isotopic characteristics of the hydrothermal system at Florence East.

6. Temperature estimates

From the sulfide and sulfate pairs, we estimated the sulfur isotopic equilibrium temperature. We also added new fluid inclusions data and compiled data from previous studies (Manalo et al., 2018, 2020) to allow comparison of the estimated temperatures (Fig. 13).

The estimated isotopic equilibrium temperatures of alunite-pyrite pairs from the Northwest area are mostly below 300 °C. Higher temperatures (greater than 350 °C) were calculated from alunite-pyrite pairs with low $\delta^{34}S$ of alunite (+15.5 and + 16.7 ‰). Manalo et al. (2018) reported fluid inclusion microthermometry data ranging from 220 to 250 °C for quartz associated with alunite, and 250 to 290 °C for quartz associated with alunite + pyrophyllite. Some samples have a wide range of homogenization temperatures due to boiling conditions and trapping of variable amounts of vapor (Manalo et al., 2018; Fig. 13). Most of the sulfur isotopic equilibrium temperatures generally agree with the range of previously reported fluid inclusion homogenization temperatures, except for the samples with low $\delta^{34}S$ of alunite with calculated isotopic equilibrium temperatures of greater than 350 °C. At temperatures above 350 °C, SO_2 rather than SO_4^{2-} becomes the dominant oxidized species (Ohmoto, 1986). The isotopic equilibrium temperature calculated using fractionation factors of SO_2 would give 210 to 220 °C, which is at the lower end of the range of homogenization temperatures and too low for SO_2 to be dominant. Thus, the fractionation factors may be between the values for SO_2 and SO_4^{2-}, indicating the possible mixing of different sulfate-bearing fluids. This observation parallels that reported by Ohmoto (1986), *i.e.,* the anhydrite and sulfide minerals in porphyry copper deposits fall within the uncalibrated area between SO_4^{2-}-H_2S and SO_2-H_2S equilibrium fractionation curves. This also applies to the sample of U-17–05 24.86 in Carmen, where the anhydrite has an exceptionally low $\delta^{34}S$ (+14.1 ‰) and an estimated sulfur isotopic equilibrium temperature of 455 °C.

In Carmen, the isotopic equilibrium temperatures of alunite-pyrite pairs range from 197 to 220 °C, while that of anhydrite-pyrite pairs range from 192 to 235 °C. Manalo et al. (2020) reported homogenization temperature of ~ 240 °C for a non-boiling fluid inclusion assemblage, while a wide range of 300 to 360 °C for the fluid inclusion assemblages with variable amounts of trapped vapor. The homogenization temperatures of fluid inclusions are generally higher than the sulfur isotopic equilibrium temperatures. In Northwest, alunite occurs along the veins, making it possible to discern which quartz crystals occur with alunite by observing textural relationship. In Carmen, the alunite crystals occur as pervasive alteration of the dacitic host rock, where remnants of porphyry-type quartz veins have been preserved (Manalo et al., 2020). It is, thus, difficult to identify which of the quartz crystals are truly coeval with alunite precipitation. It is possible that some quartz analyzed for fluid inclusions microthermometry reflect the higher temperature environment before the pervasive alunite alteration.

The sulfur isotopic equilibrium temperature of an alunite-pyrite pair from Florence West is 274 °C. There is currently no fluid inclusion data available for comparison. For Florence East, an alunite-enargite (U-16–05 172.3) and an alunite-pyrite (U-16–05 188.8) pair yielded sulfur isotopic equilibrium temperatures of 226 °C and 364 °C, respectively.

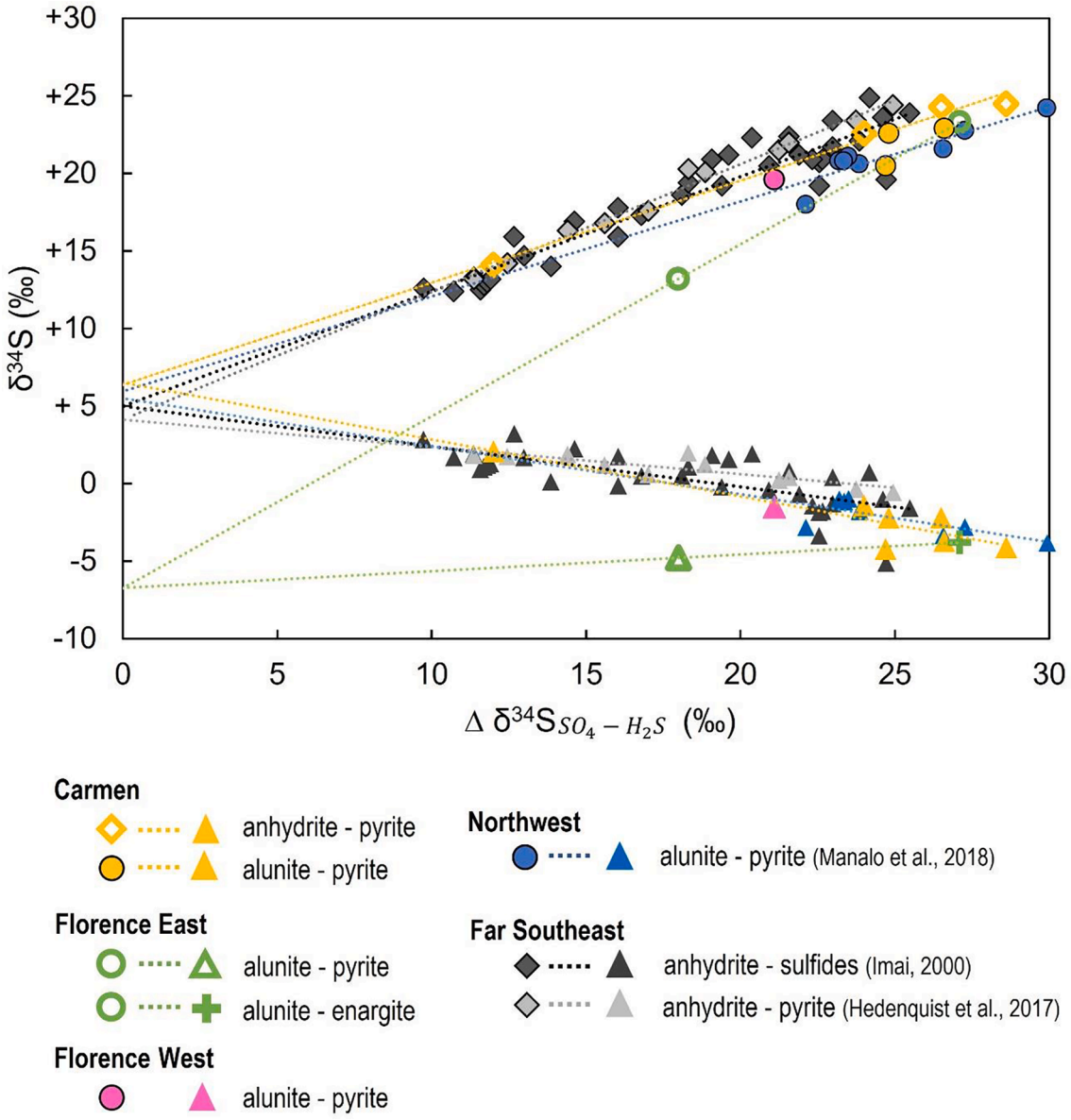

Fig. 12. $\delta^{34}S$ versus $\Delta\delta^{34}S$ [SO_4^{2-}-H_2S] diagram based on sulfate – sulfide pairs from Far Southeast (Imai, 2000; Hedenquist et al., 2017), Northwest (Manalo et al., 2018), Carmen, Florence West and Florence East. The trend of the data is similar for most of the deposits, except for an alunite-pyrite pair from the Florence East.

The modes of homogenization temperature of fluid inclusions in quartz from U-16–05 188.8 is 250 to 270 °C, close to the isotopic equilibrium temperature estimated from the alunite-enargite pair. However, the $\delta^{34}S$ of the alunite-pyrite pair of U-16–05 188.8 significantly deviated from the other sulfide-sulfate pairs in the different areas of this study. As seen in the photomicrographs (Fig. 3E and 3F), alunite and pyrite precipitated along the same vein, and they seem to have been precipitated from the same fluid. However, there are many factors that affect the $\delta^{34}S$ values of individual sulfur species, such as equilibrium fractionation factors, sulfur speciation and the isotopic composition of the total S in the fluid (Ohmoto, 1986). It is possible that more than one of these factors affected the distinctly low $\delta^{34}S$ of alunite (+13.2 ‰) from Florence East, making the calculated isotopic equilibrium temperature an invalid estimate. Watanabe and Hedenquist (2001) interpreted that the low $\delta^{34}S$ of alunite could be due to the influence of the sulfur isotopic signature of the supergene alunite that partially replaced the hypogene alunite. However, in the case of this Florence East sample which has a strikingly homogeneous chemical composition, it is unlikely that partial supergene replacement affected the isotopic composition without inducing variations in the mineral chemistry. We also did not observe replacement textures in the alunite crystals in optical and electron microscope observations.

7. Variations in Na content of alunite

We compare the mineral compositions with the sulfur isotopic ratios of the hypogene alunite in the Northwest (Fig. 14), Carmen, Florence East and Florence West areas (Fig. 15). The histograms reflect the wide variation in the amount of Na that substituted K in the alunite samples from the Northwest area. Alunites of samples U-16–118 143.6 m and U-17–01 114.4 m are richer in Na, while U-16–118 197.8 m and U-16–118 186.3 m are mostly richer in K. Alunites from samples U-16–118 109.35 m and U-16–118 175.7 m are in the intermediate composition. There is no clear trend between the Na content and the depth of the sample. We compare the Na content of the alunite with the temperatures of formation calculated using sulfur isotopic geothermometer on alunite-pyrite pairs (Supplementary Data Fig. 3). The K-rich alunites of U-16–118 186.3 m and U-16–118 197.8 m were formed at 197 °C and 277 °C,

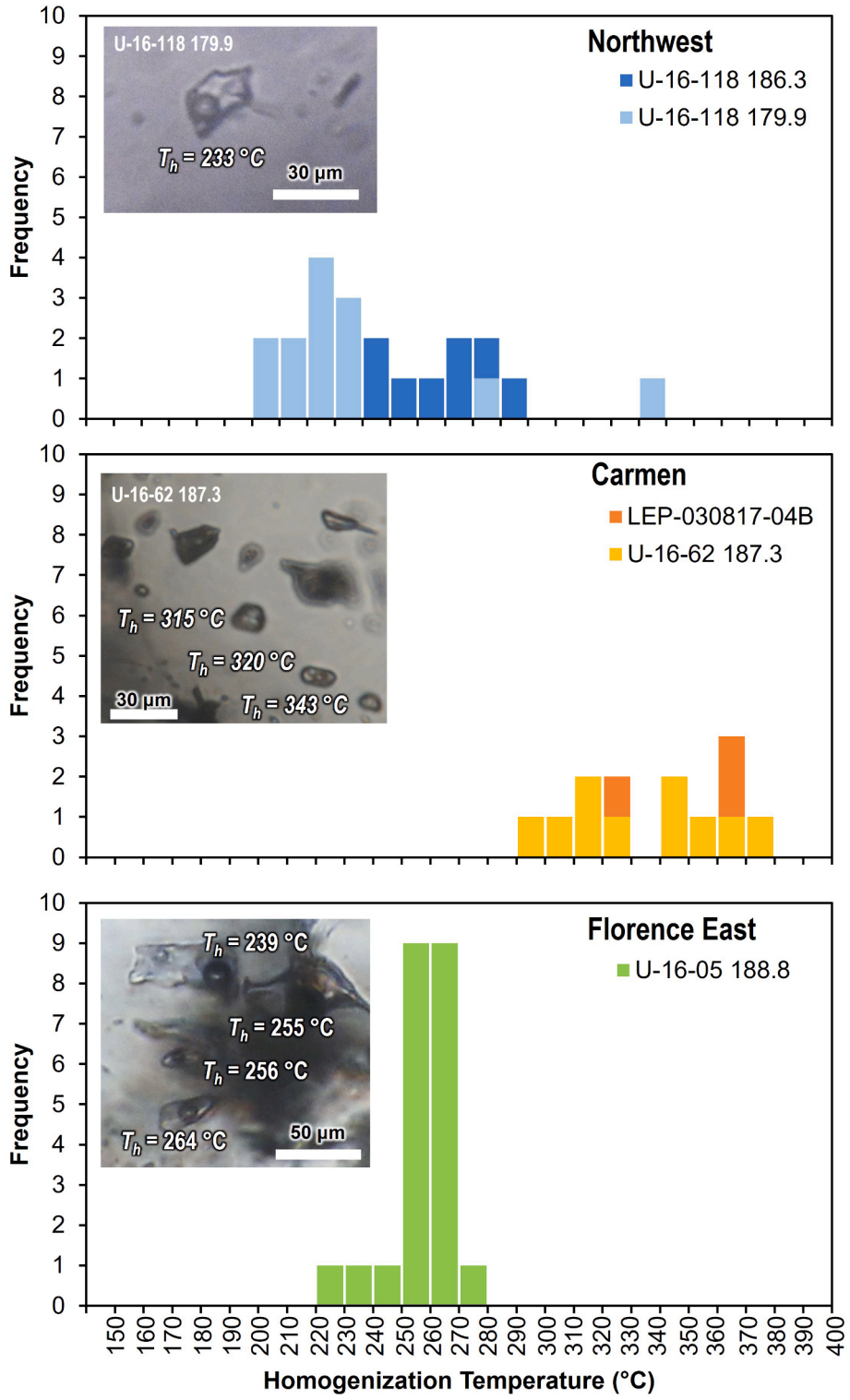

Fig. 13. Representative photomicrographs and histograms of homogenization temperatures of fluid inclusions in quartz coexisting with alunite from Northwest (Manalo et al., 2018), Carmen (Manalo et al., 2020) and Florence East.

respectively. The histograms show that the ranges of Na content of alunite in samples U-16–118 186.3 m and U-16–118 197.8 m are similar, but the temperatures calculated from the isotopic thermometry vary by 80 °C. The Na-rich alunite of U-17–01 114.4 m was formed at temperatures of around 214 °C. The formation temperatures of alunites that have intermediate Na content (U-16–118 109.35 m and U-16–118 175.7 m) are 225 °C and 271 °C, varying by about 45 °C.

The Na content of alunite from Carmen (Lep-030817-04C) exhibits wide variation and sulfur isotopic thermometry yielded a relatively low temperature of formation (197 °C). The Na contents of alunite crystals from the drillhole sample in Florence East (U-16–05 188.8 m) are remarkably uniform across different crystals, ranging between 0.4 and 0.5 apfu. Sulfur isotopic geothermometry on this sample yields a relatively high temperature of formation at 364 °C. However, the alunite-pyrite pair from this sample showed isotopic disequilibrium. Thus, a better estimate of the temperature of formation is from the

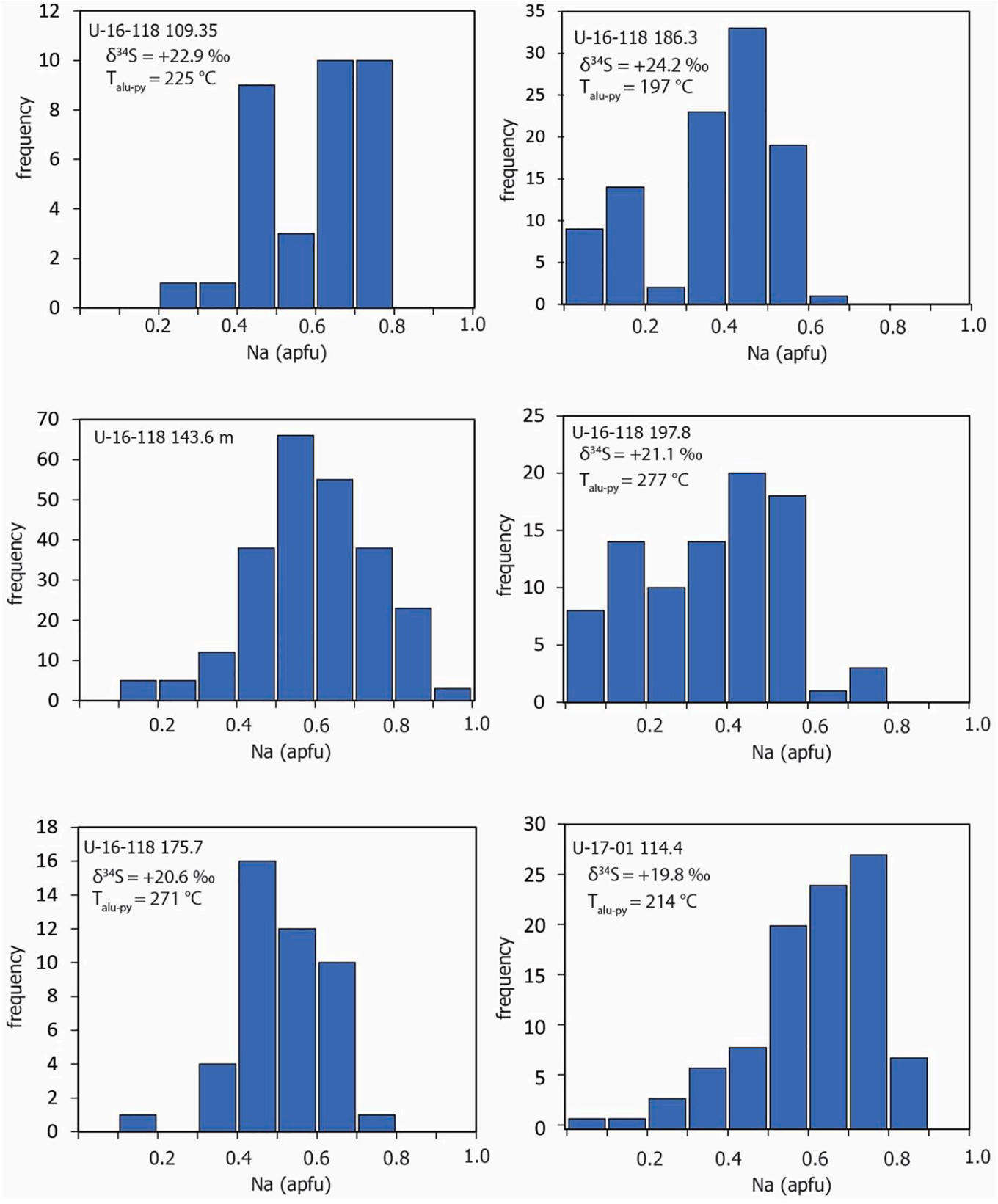

Fig. 14. Histograms showing the Na content of alunite from the different samples in the Northwest areas. The sulfur isotopic ratios of the alunites and the corresponding temperature calculated using sulfur isotope geothermometry of alunite-pyrite pairs are indicated.

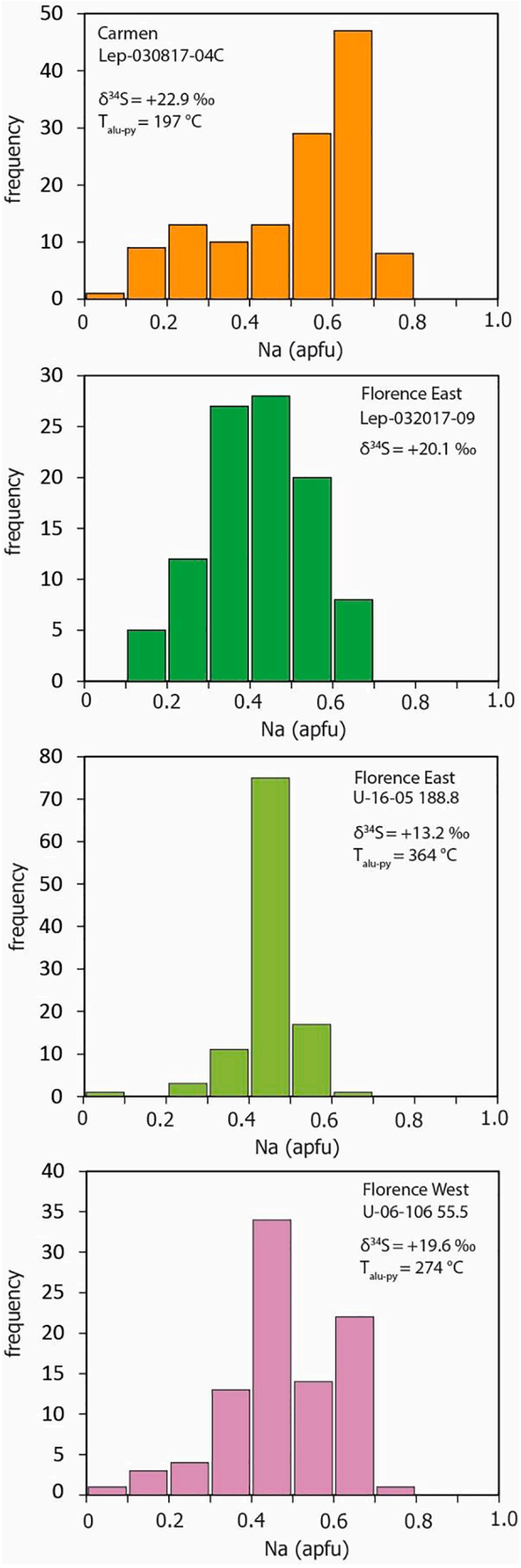

Fig. 15. Histograms showing the Na content of alunite from the Carmen, Florence East and Florence West areas. The sulfur isotopic ratios of the alunites and the corresponding temperature calculated using sulfur isotope geothermometry of alunite-pyrite pairs are indicated.

homogenization temperature of fluid inclusions in co-existing quartz (260 to 270 °C; Fig. 13). The $\delta^{34}S$ of this alunite is the lowest among all the samples measured (+13.2 ‰). Manalo et al. (2020) reported that fO_2 of hydrothermal fluids based on fluid inclusions gas analysis on quartz from Florence is higher than those from Carmen and Northwest. Changes in the oxygen fugacity would have influenced the sulfur isotopic ratios and alunite composition. The Na contents of alunite in another sample from the underground tunnels in Florence East range more widely. However, we were not able to apply the sulfur isotope geothermometer due to the very small amount of sulfides in this sample.

The Na contents of most of the alunite from the drill hole sample from Florence West (U-16–106 55.5 m) are intermediate and these alunites were formed at 274 °C. Another drillhole sample, U-16–106 67.5 m, contains only woodhouseite with the Na concentration below the detection limit. The $\delta^{34}S$ of the woodhouseite from this sample is −6.5 ‰, which is near that of the coexisting pyrite (-5.8 ‰). As discussed above, the negative $\delta^{34}S$ of this sample is not representative of the woodhouseite since APS minerals have shown resistance to NaOH dissolution (Watanabe and Hedenquist, 2001). It also shows hypogene mineral association with quartz, alunite, pyrite and enargite. The results may either be influenced by sulfide impurities or by supergene replacement.

Chang et al. (2011) reported the chemical compositions of alunite related to the Lepanto Main Enargite orebody that shows a wide range of K-Na-Ca composition (Supplementary Data Fig. 1). The K-poor alunite usually contains significant Na and Ca. Two temperature estimates were obtained using sulfur isotope geothermometer on alunite-pyrite pairs reported by Hedenquist et al. (2017). One sample (U89-34–630) yielded a temperature of formation at 218 °C and its Na content ranges from 0.3 to 0.6 apfu (Chang et al., 2011). The other sample (U91-42–156) contains alunites formed at 224 °C (Hedenquist et al., 2017) with Na content ranging from 0.2 to 0.5 apfu (Chang et al., 2011).

The general broad variations in the chemical composition of alunite and the formation temperatures indicate that the properties of the lithocap at Mankayan are not homogeneous, although it apparently occurs as a contiguous alteration zone.

7.1. Physicochemical factors affecting alunite composition

Temperature is often cited as the main controlling factor that affects Na substitution in alunite (e.g., Stoffregen and Cygan, 1990; Hedenquist et al., 2017). Deyell (2001) and Deyell and Dipple (2005) illustrated that the composition of the hydrothermal fluid also affects the degree of Na substitution in alunite. Using thermodynamic relationships, we investigated how the temperature and fluid composition vary among the alunite in the lithocap at Mankayan.

The equilibrium between a solid solution and an aqueous solution of its ions have been earlier presented by Berndt and Stearns (1973) and Glynn and Reardon (1990). For the consistency of representation, we follow Deyell and Dipple (2005) in expressing the equilibrium constant of the substitution reaction (1) as:

$$\left(\frac{a_{K^+}}{a_{Na^+}}\right)_{fluid} = K_1\left[\frac{a_{Kaln,\,s}}{a_{Naln,s}}\right] \tag{6}$$

where a_{Na^+} and a_{K^+} refer to the activities of Na^+ and K^+ in the hydrothermal solution, respectively, and K_1 is the equilibrium constant of reaction (1). The parameters $a_{Kaln,s}$ and $a_{Naln,s}$ are the activities of alunite and natroalunite in the mineral, respectively. The activities of alunite and natroalunite in the solid solution can be calculated using the formula (7a) and (7b), respectively,

$$a_{Kaln,s} = X_{Kaln,s}\,\gamma_{Kaln} \tag{7a}$$

$$a_{Naln,s} = X_{Naln,s}\,\gamma_{Naln} \tag{7b}$$

where $X_{Kaln,s}$ and $X_{Naln,s}$ are the mole fractions of alunite and

natroalunite in the solid solution, respectively. The parameters γ_{Kaln} and γ_{Naln} are the activity coefficients of alunite and natroalunite at a specific temperature. For solid solutions, a subregular Margules mixing model can be used to determine the respective activity coefficient of alunite and natroalunite (Stoffregen and Cygan, 1990) following the formula:

$$RTln\gamma_{Kaln} = (2W_{GNaln} - 2W_{GKaln})X^2_{Naln} + 2(2W_{GKaln} - 2W_{GNaln})X^2_{Kaln} \quad (8)$$

where W_{GKaln} and W_{GNaln} are the mixing parameters for alunite and natroalunite, respectively (Anderson and Crerar, 1993). These mixing parameters have been determined by Stoffregen and Cygan (1990) at temperatures of 250, 350 and 450 °C. The mixing parameters at different temperatures were estimated by least squared regression of the published W_{GKaln} and W_{GNaln} data (Stoffregen and Cygan, 1990; Deyell, 2001). From these equations, the activities of alunite and natroalunite in solid solution can be determined.

The equilibrium constant, K_1, was calculated at different temperatures using the R package CHNOSZ (Dick, 2019) using the OBIGT thermodynamic database, which includes alunite and natroalunite thermodynamic data recommended by Stoffregen et al. (2000). We added the molar volume data of natroalunite determined by Stoffregen and Cygan (1990). The calculations were performed assuming that pressure is 500 bars. Deyell (2001) previously illustrated that pressure variations do not significantly affect the calculation results. After determining the K_1 at different temperatures, we calculated the $\left(\frac{a_{K^+}}{a_{Na^+}}\right)_{fluid}$ at varying compositions of alunite – natroalunite solid solution. From here, the model curves depicting the relationships of temperature and fluid compositions were constructed (Fig. 16).

The model curves show that at temperatures below 250 °C, the K content of the alunite-natroalunite solid solution can vary from 0.3 apfu to 0.6 apfu within a narrow range of $(a_{K^+}/a_{Na^+})_{fluid}$ values. This means that a very little change in fluid composition at constant temperature can result a variable degree of Na substitution of alunite below 250 °C. Conversely, a slight increase in temperature within the range from 200 to 250 °C at a constant fluid composition can vary the Na content of alunite by as much as 0.3 apfu. At higher temperatures, the model curves are more far apart from each other, indicating that a considerable change in fluid composition is necessary for Na^+ substitution of alunite. The model curves also suggest that the end members of the solid solution can be formed from fluids with either significantly low or significantly high K^+ concentration. If the K^+/Na^+ ratios of fluids vary within the $1*10^{-1}$ order of magnitude, a slight change in temperature (~50 °C) and/or fluid composition can change the Na content of alunite by 0.3 apfu.

This explains why a wide range of compositions within a single sample, as seen in the histograms of the Na content of alunite (Figs. 14 and 15), is common in the samples from the lithocap at Mankayan. The heterogeneity within a single crystal of alunite suggests local fluctuation in the temperature and fluid composition. Similar compositional variation of alunite in lithocaps has also been observed in other deposits (Supplementary Data Fig. 4). A wide range of alunite-natroalunite solid solution in the Cerro Quema high-sulfidation Au-Cu deposit, Panama (Corral et al., 2016) was reported to have an average sulfur isotopic equilibrium temperature of 239 °C (Corral et al., 2017). A wide range of Na content of alunite was also reported from Chelopech, Bulgaria (Georgieva et al., 2020) and from Konos Hill, Greece (Mavrogonatos et al., 2018), although no direct comparison to temperature has been made.

Deyell et al. (2005) documented different types of alunite in the Tambo high-sulfidation deposit, Chile, which also exhibit wide range of compositions. The Stage 1 magmatic-hydrothermal alunite in Tambo has been described to be chemically heterogeneous and has the highest average Na content in the deposit (average Na content = 0.19 apfu, maximum = 0.81 apfu; Deyell et al., 2005). They reported an unusual wide range of $\delta^{34}S$ from + 1 ‰ to + 23 ‰ and a temperature of

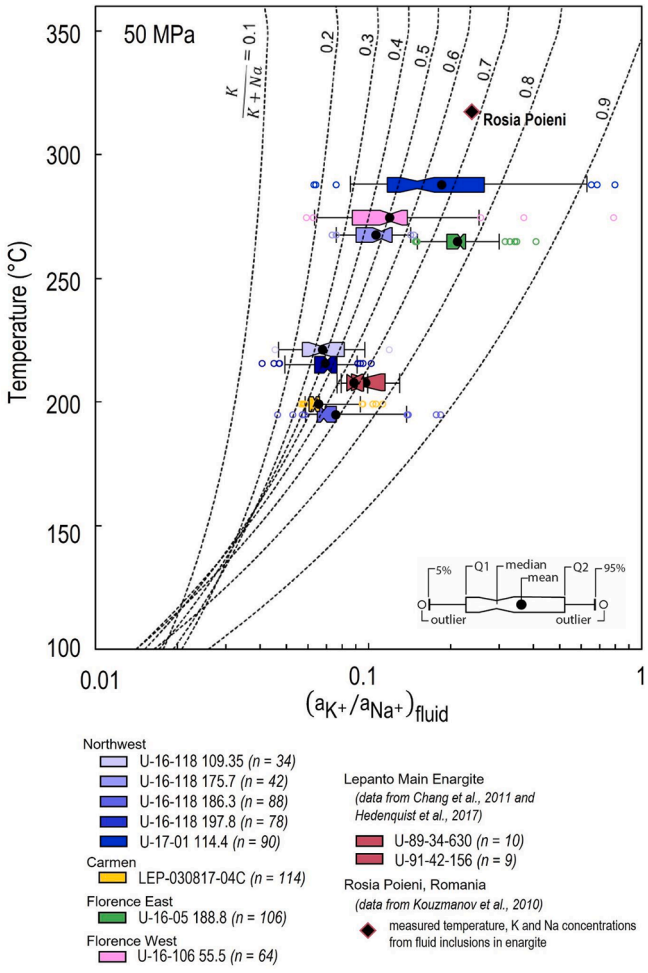

Fig. 16. Relationship between temperature and activity ratios of K^+ and Na^+ in the hydrothermal fluid across varying composition of the alunite-natroalunite solid solution. The dashed lines with numbers indicate the K/(K + Na) mole fraction of alunite in the solid solution. The range of K/Na activity ratios of fluids were calculated for the Northwest, Carmen and Florence West areas using the temperature from sulfur isotope geothermometer of alunite-pyrite pairs and composition of alunite measured by the electron probe microanalyzer. The temperature used for Florence East was from the homogenization temperature of fluid inclusions. Data from Chang et al. (2011) and Hedenquist et al. (2017) were used to plot the range for the Lepanto Main Enargite orebody. The K^+/Na^+ activity ratios of fluids of the Rosia Poieni deposit was calculated from the concentration of the fluid inclusions in enargite reported by Kouzmanov et al. (2010). The temperature of the Rosia Poieni deposit was obtained by microthermometry of fluid inclusions in enargite (Kouzmanov et al., 2010).

deposition from 200 to 280 °C (Deyell et al., 2005). On the other hand, Stage 2 of the Tambo deposit has Na-poor (less than0.2 apfu) but Ba-rich alunite and shows a nearly complete solid solution composition between alunite and walthierite (Deyell et al., 2005). The $\delta^{34}S$ of alunite ranges from + 26 to + 27 ‰ with a calculated depositional temperature of 180 to 250 °C based on the $\Delta^{18}O_{SO4\text{-}OH}$, which is the isotopic fractionation of ^{18}O between the SO^4 and OH of alunite (Deyell et al., 2005). There are no reported chemical composition of alunite with a formation temperature greater than 300 °C. Hedenquist et al. (2017) reported sulfur isotopic equilibrium temperature of up to 411 °C for alunite-pyrite pairs near the Far Southeast deposit, but no corresponding mineral chemistry is available. It would be interesting to see the chemical compositions of these very high temperature alunite in future studies.

We calculated the estimated range of fluid composition of the hydrothermal fluid (Fig. 16) using the measured chemical composition of alunite in the lithocap at Mankayan and the temperature calculated from

the sulfur isotopic thermometry on alunite-pyrite pairs. For the sample from Florence East (U-16–05 188.8), we used the homogenization temperature of fluid inclusions in quartz for the calculations, since the alunite-pyrite pair showed sulfur isotopic disequilibrium (Fig. 12). The ratios of the activities of K^+ and Na^+ of the fluid vary from 0.05 to 0.2. The plot reflects that alunite from the different parts of the lithocap in Mankayan formed in conditions with varying temperature and fluid composition.

The absence of hydrothermal fluid composition data in the Mankayan District precludes the direct comparison of the calculated K^+/Na^+ ratios with actual measurements. However, Kouzmanov et al. (2010) measured the element concentrations of the fluid in enargite-hosted fluid inclusions of the Rosia Poieni deposit, Romania using LA-ICPMS. Alunite also occurs in the Rosia Poieni deposit, which makes it a good area for comparison. We used the measured Na and K concentration of the fluids trapped in enargite crystals (Kouzmanov et al., 2010) to represent the possible composition of fluids in the high-sulfidation epithermal environment. The average Na and K concentration of the fluid inclusions hosted in enargite at Rosia Poieni are 2634 ppm and 1164 ppm, respectively (Kouzmanov et al., 2010). Using the Truesdell – Jones equation, we calculated the activity coefficient of Na^+ and K^+ at 317 °C, using the homogenization temperature of fluid inclusions hosted in enargite reported by Kouzmanov et al. (2010) and ionic strength determined at 0.2 M chlorinity and 0.01 M sulfate concentration (Deyell, 2001). The calculated $\left(\frac{a_{K^+}}{a_{Na^+}}\right)_{fluid}$ of the fluid inclusion hosted in enargite from Rosia Poieni is 0.25. Kouzmanov et al (2010) noted the restricted range of K/Na ratios in the hydrothermal fluids in Rosia Poieni, which was due to the overprinting of epithermal event onto earlier potassic or phyllic alteration.

Thermodynamic relationships indicate a close interplay between temperature and fluid composition in determining the composition of the alunite – natroalunite solid solution system. The composition of the host rocks is also a key factor in determining the alunite composition because it affects mineral stability during water–rock interaction. Alunite in Mankayan, as well as in other lithocaps associated with Au and Cu mineralization, is commonly heterogeneous even at microscopic scale. Thus, caution is required in using alunite and natroalunite as regional vectors for mineralization.

8. Conclusions

This study reported the variations in the mineral chemistry and sulfur isotopic ratios of alunite in the lithocap at Mankayan, which hosts high-sulfidation epithermal gold orebodies in the Northwest, Carmen, Florence East and Florence West areas. Alunite crystals occur as interstitial to vein quartz, or as pervasive alteration of the host rock. Elemental composition maps indicate the heterogeneity of mineral composition within a single crystal and among interlocking alunite crystals. Sodium substitution varies widely, while Ca and hydronium substitute to some extent.

Sulfur isotopic ratios ($\delta^{34}S$) of the hypogene alunites mostly vary from + 13 ‰ to + 24 ‰. The $\delta^{34}S$ of few alunite and APS mineral samples from Northwest and Florence West are negative, which is similar to those of the coexisting pyrite. The bulk $\delta^{34}S$ of the hydrothermal fluid that formed the lithocap in Carmen is + 6 ‰, similar to the values previously reported for the Northwest and the Far Southeast deposits. This indicates that across the different mineralization events, the bulk isotopic composition of the fluid is broadly identical.

Most of the calculated isotopic equilibrium temperatures vary between 220 and 270 °C, which correspond to the homogenization temperature of fluid inclusions in quartz. Anomalously high isotopic equilibrium temperatures (greater than 350 °C) and low $\delta^{34}S$ are likely a product of sulfate-bearing fluids that differs from the fractionation behavior of the SO_4-H_2S system.

The variation in the extent of Na and Ca substitution are not strongly correlated with temperature. The variable composition of alunites reflects the fluctuating temperature conditions and fluid composition throughout the mineralization in the Mankayan District.

Declaration of Competing Interest

The authors declare that they have no known competing financial interests or personal relationships that could have appeared to influence the work reported in this paper.

Acknowledgements

We thank Mr. Bryan Yap, president of the Lepanto Consolidated Mining Co., for allowing us to publish the results of this study. We are grateful to the exploration geology and mine geology team of Lepanto Consolidated Mining Co. for their logistical and technical support. Financial support was provided by the Akita University New Frontier Leaders for Rare-Metals and Resources program for fieldwork and laboratory analyses. Additional financial support was provided by the Japan Society for the Promotion of Science (JSPS) Grants-in-Aid for Scientific Research (17K06982, 21K04960, 21KK0089). Part of the data used in this study was acquired when P. Manalo was being supported by a Japanese Monbukagakusho Scholarship. We thank Hinako Sato, Hertz Balmater, Jonathan Macuroy and Enrico Suharjo for the assistance in the laboratory analyses and sample preparation. We also thank Andrea Agangi for software support and his suggestions to the manuscript. We are immensely grateful to Huayong Chen, Alain Chauvet, Isaac Corral and an anonymous reviewer for their constructive reviews that improved the manuscript. Discussions with the members of the Economic Geology Research Groups, Akita University are highly appreciated.

Appendix A. Supplementary data

Supplementary data to this article can be found online at https://doi.org/10.1016/j.oregeorev.2022.104959.

References

Amante, C., Eakins, B.W., 2009. ETOPO1 Arc-Minute Global Relief Model: Procedures, Data Sources and Analysis. NOAA Technical Memorandum NESDIS NGDC-24.
Anderson, G.M., Crerar, D.A., 1993. Thermodynamics in Geochemistry. Oxford University Press, New York, The Equilibrium Model.
Arribas, A., Cunningham, C.G., Rytuba, J.J., Rye, R.O., Kelly, W.C., Podwysocki, M.H., McKee, E.H., Tosdal, R.M., 1995a. Geology, geochronology, fluid inclusions, and isotope geochemistry of the Rodalquilar gold alunite deposit, Spain. Economic Geology 90, 795–822.
Arribas, A., Hedenquist, J.W., Itaya, T., Okada, T., Concepcion, R., Garcia Jr., J.S., 1995b. Contemporaneous formation of adjacent porphyry and epithermal Cu-Au deposits over 300 ka in northern Luzon, Philippines. Geology 23, 337–340.
Audétat, A., 2019. The metal content of magmatic-hydrothermal fluids and its relationship to mineralization potential. Economic Geology 114, 1033–1056.
Back, M., 2014. Fleischer's Glossary of Mineral Species, 11th ed. Mineralogical Record Inc., Tucson.
Bayliss, P., Kolitsch, U., Nickel, E.H., Pring, A., 2010. Alunite supergroup: recommended nomenclature. Mineralogical Magazine 74, 919–927.
Benison, K.C., Bowen, B.B., Oboh-Ikuenobe, F., Jagniecki, E.A., LaClair, D.A., Story, S.L., Mormile, M.R., Hong, B.Y., 2007. Sedimentology of acid saline lakes in Southern Western Australia: Newly described processes and products of an extreme environment. Journal of Sedimentary Research 77, 366–388.
Berndt, A.F., Stearns, R.I., 1973. The equilibrium between a solid solution and an aqueous solution of its ions. Journal of Chemical Education 50, 415–417.
Bethke, P.M., Rye, R.O., Stoffregen, R.E., Vikre, P.G., 2005. Evolution of the magmatic-hydrothermal acid-sulfate system at Summitville, Colorado; Integration of geological, stable isotope, and fluid inclusion evidence. Chemical Geology 215, 281–315.
Beudant, F.S., 1824. 22e espèce. Alunite. In, Traité élémentaire de Minéralogie, A Paris, pp. 449–450.
Chambefort, I., Moritz, R., 2014. Subaqueous environment and volcanic evolution of the Late Cretaceous Chelopech Au-Cu epithermal deposit, Bulgaria. Journal of Volcanology and Geothermal Research 289, 1–13.
Chang, Z., Hedenquist, J.W., White, N.C., Cooke, D.R., Roach, M., Deyell, C.L., Garcia Jr., J., Gemmell, J.B., McKnight, S., Cuison, A.L., 2011. Exploration tools for

linked porphyry and epithermal deposits: Example from the Mankayan intrusion-centered Cu-Au district, Luzon, Philippines. Economic Geology 106, 1365–1398.
Claveria, R.J., 2001. Mineral paragenesis of the Lepanto copper and gold and the Victoria gold deposits, Mankayan mineral district, Philippines. Resource Geology 51, 97–106.
Cooke, D.R., Wilson, A.J., Davies, A.G.S., 2004. Characteristics and genesis of porphyry copper-gold deposits. University of Tasmania, Center for Ore Deposit Research, Special Publication 5, 17–34.
Corral, I., Cardellach, E., Corbella, M., Canals, A., Gómez-Graz, D., Griera, A., Cosca, M., 2016. Cerro Quema (Azuero Peninsula, Panama): Geology, alteration, mineralization, and geochronology of a volcanic dome-hosted high-sulfidation Au-Cu deposit. Economic Geology 111, 287–310.
Corral, I., Cardellach, E., Corbella, M., Canals, A., Griera, À., Gómez-Gras, D., Johnson, C. A., 2017. Origin and evolution of mineralizing fluids and exploration of the Cerro Quema Au-Cu deposit (Azuero Peninsula, Panama) from a fluid inclusion and stable isotope perspective. Ore Geology Reviews 80, 947–960.
Deyell, C.L., 2001. Alunite and High Sulfidation Gold-Silver-Copper Mineralization in the El Indio-Pascua Belt, Chile-Argentina. PhD Dissertation. University of British Columbia, Vancouver, Canada.
Deyell, C.L., Dipple, G.M., 2005. Equilibrium mineral-fluid calculations and their application to the solid solution between alunite and natroalunite in the El Indio-Pascua belt of Chile and Argentina. Chemical Geology 215, 219–234.
Deyell, C.L., Rye, R.O., Landis, G.P., Bissig, T., 2005. Alunite and the role of magmatic fluids in the Tambo high-sulfidation deposit, El Indio-Pascua belt, Chile. Chemical Geology 215, 185–218.
Dick, J.M., 2019. CHNOSZ: Thermodynamic calculations and diagrams for geochemistry. Frontiers in Earth Science. https://doi.org/10.3389/feart.2019.00180.
Ehlmann, B.L., Swayze, G.A., Milliken, R.E., Mustard, J.F., Clark, R.N., Murchie, S.L., Breit, G.N., Wray, J.J., Gondet, B., Poulet, F., Carter, J., Calvin, W.M., Benzel, W.M., Seelos, K.D., 2016. Discovery of alunite in Cross crater, Terra Sirenum, Mars: Evidence for acidic, sulfurous waters. American Mineralogist 101, 1527–1542.
Field, C., 1966. Sulfur isotopic method for discriminating between sulfates of hypogene and supergene origin. Economic Geology 61, 1428–1435.
Field, C.W., Gustafson, L.B., 1976. Sulfur isotopes in the porphyry copper deposit at El Salvador, Chile. Economic Geology 71, 1533–1548.
Garcia, J.S., Bongolan, M.B., 1989. Developments in enargite ore search at Lepanto. Mankayan, Benguet, Philippines: Geological Survey of Japan, Report 277, 21–30.
Georgieva, S., Stefanova, E., Hikov, A., Peytcheva, I., 2020. Trace element geochemistry of alunite from the Chelopech high-sulfidation epithermal deposit, Bulgaria: A potential tool for exploration of epithermal deposits. Comptes Rendus de L'Academie Bulgare des Sciences 73, 1092–1101.
Giggenbach, W.F., 1997. The origin and evolution of fluids in magmatic-hydrothermal systems. In: Barnes, H.L. (Ed.), Geochemistry of Hydrothermal Ore Deposits, 3rd ed. John Wiley & Sons Inc, New York, pp. 737–795.
Glynn, P.D., Reardon, E.J., 1990. Solid-solution aqueous solution equilibria: Thermodynamic theory and representation. American Journal of Science 290, 164–201.
Goldberry, R., 1980. Early diagenetic, Na-alunites in Miocene algal mat intertidal facies, Ras Sudar, Sinai. Sedimentology 27, 189–198.
Halas, S., Szaran, J., 2001. Improved thermal decomposition of sulfates to SO_2 and mass spectrometric determination of $\delta^{34}S$ of IAEA SO-5, IAEA SO-6, and NBS-127 sulfate standards. Rapid communications in Mass Spectrometry 15, 1618–1620.
Hayba, D.O., Bethke, P.M., Heald, P., Foley, N.K., 1986, Geologic, mineralogic and geochemical characteristics of volcanic-hosted epithermal precious metal deposits. In Berger, B.R., Bethke, P.M. (eds.) Geology and Geochemistry of Epithermal Systems. Reviews in Economic Geology, 2, 129-167.
Hedenquist, J.W., Arribas, A., 2022. Exploration implications of multiple formation environments of advanced argillic minerals. Economic Geology 117, 609–643.
Hedenquist, J.W., Claveria, R.J.R., Villafuerte, G.P., 2001, Types of sulfide-rich epithermal deposits, and their affiliation to porphyry systems: Lepanto-Victoria-Far Southeast deposits, Philippines, as examples. Conference Proceedings. ProExplo Congreso, Lima, Peru, 24-28 April 2001, p. 29.
Hedenquist, J.W., Arribas Jr., A., Aoki, M., 2017. Zonation of sulfate and sulfide minerals and isotopic composition in the Far Southeast porphyry and Lepanto epithermal Cu-Au deposits, Philippines. Resource Geology 67, 174–196.
Hemley, J.J., Hostetler, P.B., Gude, J., Mountjoy, W.T., 1969. Some stability relations of alunite. Economic Geology 64, 599–612.
Hladky, G., Slansky, E., 1981. Stability of alunite minerals in aqueous solutions at normal temperature and pressure. Bulletin de Mineralogie 104, 468–477.
Hutchison, W., Finch, A., Boyce, A.J., 2020. The sulfur isotope evolution of magmatic-hydrothermal fluids: insights into ore-forming processes. Geochimica et Cosmochimica Acta 288, 176–198.
Imai, A., 2000. Mineral paragenesis, fluid inclusions and sulfur isotope systematics of the Lepanto Far Southeast Porphyry Cu-Au deposit, Mankayan, Philippines. Resource Geology 50, 151–168.
Jambor, J.L., 1999. Nomenclature of the alunite supergroup. The Canadian Mineralogist 37, 1323–1341.
Jimenez, F.A., Yumul Jr., G.P., Maglambayan, V.B., Tamayo Jr., R.A., 2002. Shallow to near-surface, vein-type epithermal gold mineralization at Lalab in the Sibutad gold deposit, Zamboanga del Norte, Mindanao, Philippines. Journal of Asian Earth Sciences 21, 119–133.
Kouzmanov, K., Pettke, T., Heinrich, C.A., 2010. Direct analysis of ore-precipitating fluids: combined IR Microscopy and LA-ICP-MS study of fluid inclusions in opaque ore minerals. Economic Geology 105, 351–373.
Lerouge, C., Kunov, A., Fléhoc, C., Georgieva, S., Hikov, A., Lescuyer, J., Petrunov, R., Velinova, N., 2006. Constraints of stable isotopes on the origin of alunite from advanced argillic alteration systems in Bulgaria. Journal of Geochemical Exploration 90, 166–182.
Long, D.T., Fegan, N.E., McKee, J.D., Lyons, W.B., Hines, M.E., Macumber, P.G., 1992. Formation of alunite, jarosite and hydrous iron oxides in a hypersaline system: Lake Tyrrell, Victoria, Australia. Chemical Geology 96, 183–202.
Manalo, P.C., Imai, A., Subang, L., de los Santos, M., Yanagi, K., Takahashi, R., Blamey, R., 2018, Mineralization of the northwest quartz-pyrite-gold veins: Implications for multiple mineralization events at Lepanto, Mankayan Mineral District, northern Luzon, Philippines. Economic Geology, 113, 1609-1626.
Manalo, P.C., Subang, L.L., Imai, A., de los Santos, M.C., Takahashi, R., Blamey, N.J.F., 2020, Geochemistry and fluid inclusions analysis of vein quartz in the multiple hydrothermal systems of the Mankayan Mineral District, Philippines. Resource Geology, 70, 1-27.
Mavrogonatos, C., Voudouris, P., Spry, P., Melfos, V., Klemme, S., Berndt, J., Baker, T., Moritz, R., Bissig, T., Monecke, T., Zaccarini, F., 2018. Mineralogical study of the advanced argillic alteration zone at the Konos Hill Mo-Cu-Re-Au porphyry prospect. NE Greece. Minerals 8, 479–496.
Moss, A.A., 1958. Alumian and natroalunite. Mineralogical Magazine 31, 884–885.
Ohmoto, H., 1986. Stable isotope geochemistry of ore deposits. Reviews in Mineralogy 16, 491–560.
Ohmoto, H., Goldhaber, M., 1997. Isotopes of sulfur and carbon. In: Barnes, H.L. (Ed.), Geochemistry of Hydrothermal Ore Deposits, 3rd ed. Wiley, New York, pp. 517–611.
Ohmoto, H., Lasaga, A., 1982. Kinetics of reactions between aqueous sulfates and sulfides in hydrothermal systems. Geochimica et Cosmochimica Acta 46, 1727–1745.
Ohmoto, H., Rye, R.O., 1979. Isotopes of sulfur and carbon. In: Barnes, H.L. (Ed.), Geochemistry of Hydrothermal Ore Deposits, 2nd ed. Wiley, New York, pp. 509–567.
Palache, C., Berman, H., Frondel, C., 1951, The System of Mineralogy of James Dwight Dana and Edward Salisbury Dana, Yale University 1837-1892, Volume II. John Wiley and Sons, Inc., New York, 7th ed., Revised and Enlarged, 1124p.
Papike, J., Karner, J., Spilde, M., Shearer, C., 2006. Terrestrial analogs of martian sulfates: Major and minor element systematics of alunite-jarosite from Goldfield. Nevada. American Mineralogist 91, 1197–1200.
Parker, R.L., 1962. Isomorphous substitution in natural and synthetic alunite. American Mineralogist 47, 127–136.
Rye, R.O., 2005. A review of the stable-isotope geochemistry of sulfate minerals in selected igneous environments and related hydrothermal systems. Chemical Geology 215, 5–36.
Rye, R.O., Bethke, P.M., Wasserman, M.D., 1991. The Stable Isotope Geochemistry of Acid-sulfate Alteration and Vein Forming Alunite. U.S. Geological Survey Open-File Report 91–257.
Rye, R.O., Bethke, P.M., Wasserman, M.D., 1992. The stable isotope geochemistry of acid sulfate alteration. Economic Geology 87, 225–262.
Sahlström, F., Dirks, P., Chang, Z., Arribas, A., Corral, I., Obiri-Yeboah, M., Hall, C., 2018. The Paleozoic Mount Carlton Deposit, Bowen Basin, Northeast Australia: Shallow high-sulfidation epithermal Au-Ag-Cu mineralization formed during rifting. Economic Geology 113, 1733–1767.
Sahlström, F., Chang, Z., Arribas, A., Dirks, P., Johnson, C.A., Huizenga, J.M., Corral, I., 2020. Reconstruction of an Early Permian, sublacustrine magmatic-hydrothermal system: Mount Carlton epithermal Au-Ag-Cu deposit, northeastern Australia. Economic Geology 115, 129–152.
Sajona, F.G., Izawa, E., Motomura, Y., Imai, A., Sakakibara, H., Watanabe, K., 2002. Victoria carbonate-base metal gold deposit and its significance in the Mankayan Mineral District, Luzon. Philippines. Resource Geology 52, 315–328.
Sakai, H., 1968. Isotopic properties of sulfur compounds in hydrothermal processes. Geochemical Journal 2, 29–40.
Sakai, H., Matsubaya, O., 1977. Stable isotopic studies of Japanese geothermal systems. Geothermics 5, 97–124.
Sakakibara, F., Sajona, F.F., Cuncan, R.A., Watanabe, K., Izawa, E., 2001. In: Hydrothermal alteration and mineralization age of the Victoria gold deposit, Mankayan Mineral District, Philippines. Kyushu University, Fukuoka, Japan, Proceedings, pp. 71–76.
Schoch, A.E., Beukes, G.J., van der Westhuizen, W.A., de Bruiyn, H., 1989. Natroalunite from Koenabib, Pofadder district, South Africa. South African Journal of Geology 92, 20–28.
Scott, K.M., 1987. Solid solution in, and classification of, gossan-derived members of the alunite-jarosite family, northwest Queensland, Australia. American Mineralogist 72, 178–187.
Scott, K.M., 1992. Origin of alunite- and jarosite-group minerals in the Mt. Leyshon epithermal gold deposit, northeast Queensland, Australia – Reply. American Mineralogist 77, 860–862.
Sillitoe, R.H., Angeles, Jr., C.A., 1985, Geological characteristics and evolution of a gold-rich porphyry copper deposit at Guinaoang, Luzon, Philippines [abs.]: Institute of Mining and Metallurgy, Asian Mining, London, 1985, Abstract Volume, p. 15–26.
Stoffregen, R.E., Alpers, C.N., 1992. Observations on the unit cell parameters, water contents and δD of natural and synthetic alunites. American Mineralogist 77, 1092–1098.
Stoffregen, R.E., Cygan, G.L., 1990. An experimental study of Na-K exchange between alunite and aqueous sulfate solutions. American Mineralogist 75, 209–220.
Stoffregen, R.E., Alpers, C.N., Jambor, J.L., 2000. Alunite-jarosite crystallography, thermodynamics, and geochronology. Reviews in Mineralogy and Geochemistry 40, 453–479.
Subang, L.L., 2017, Geology and Geochemistry of the Quartz-Pyrite-Gold High Sulfidation Epithermal Au + Ag ± Cu Veins, Mankayan Mineral District, Northern Luzon, Philippines: M.Sc. Thesis, Hobart, Australia, University of Tasmania, 205p.

Voudouris, P., 2011. Conditions of formation of the Mavrokoryfi high-sulfidation epithermal Cu-Ag-Au-Te mineralization (Petrota Graben, NE Greece). Mineralogy and Petrology 101, 97–113.
Watanabe, Y., Hedenquist, J.W., 2001. Mineralogic and stable isotope zonation at the surface over the El Salvador porphyry copper deposit, Chile. Economic Geology 96, 1775–1797.
White, D.E., Hem, J.D., Waring, G.A., 1963. Chemical Composition of Subsurface Waters. United States Geological Survey Professional Paper 440-L, 67p.
Whitney, D., Evans, B.W., 2010. Abbreviation for names of rock-forming minerals. American Mineralogist 95, 185–187.
Wise, W.S., 1975. Solid solution between the alunite, woodhouseite and crandallite mineral series. Neues Jahrbuch fur Mineralogie Monastshefte 540–545.